Hindawi
Geofluids
Volume 2017, Article ID 4358985, 32 pages
https://doi.org/10.1155/2017/4358985

Research Article

Reconstruction of the Cenozoic History of Hydrocarbon Fluids from Rifting Stage to Passive Continental Margin Stage in the Huizhou Sag, the Pearl River Mouth Basin

Yajun Li,[1,2] Shu Jiang,[3] Zhenglong Jiang,[1] Hao Liu,[1] and Bingxi Li[4]

[1]*School of Marine Sciences, China University of Geosciences, Beijing 100083, China*
[2]*School of Energy Resources, China University of Geosciences, Beijing 100083, China*
[3]*Energy and Geoscience Institute, University of Utah, Salt Lake City, UT 84108, USA*
[4]*Beijing Ultron Era Scientific Co., Ltd., Beijing 100080, China*

Correspondence should be addressed to Shu Jiang; sjiang@egi.utah.edu and Zhenglong Jiang; jiangzl@cugb.edu.cn

Received 5 May 2017; Revised 28 August 2017; Accepted 3 October 2017; Published 21 November 2017

Academic Editor: Stefano Lo Russo

Copyright © 2017 Yajun Li et al. This is an open access article distributed under the Creative Commons Attribution License, which permits unrestricted use, distribution, and reproduction in any medium, provided the original work is properly cited.

The Eocene lacustrine sediments are the primary source rocks in the Huizhou Sag of the Pear River Mouth Basin. This study employs basin modeling for four representative wells and two profiles in the Huizhou Sag to reconstruct the process of generation, expulsion, migration, and accumulation of hydrocarbon fluids. The Eocene source rocks started to generate hydrocarbon at 33.9 Ma and are currently in a mid-mature and postmature stage. Hydrocarbons are mainly expelled from the Eocene Wenchang Fm, and the contribution of the Eocene Enping formation is minor. Under the driving forces of buoyancy and excess pressure, major hydrocarbons sourced from the Eocene source rocks firstly migrated laterally to the adjacent Eocene reservoirs during the postrift stage, then vertically via faults to Oligo-Miocene carrier beds, and finally laterally to the structural highs over a long distance during the Pliocene-Quaternary Neotectonic stage, which is controlled by both structural morphology and heterogeneity of carrier beds. Fault is the most important conduit for hydrocarbon fluid migration during the Neotectonic stage. Reactivation of previous faults and new-formed faults caused by the Dongsha Movement (9.8–4.4 Ma) served as vertical migration pathways after 10.0 Ma, which significantly influenced the timing of hydrocarbon accumulation in the postrift traps.

1. Introduction

As the largest basin in the northern continental margin of the South China Sea (SCS), the Pearl River Mouth Basin (PRMB) has become the exploration focus due to a series of hydrocarbon discoveries. Hydrocarbon exploration in the PRMB began in 1973, and reservoirs were successively found in several hydrocarbon generation sags. According to the existing commercial discoveries, the northern basins located in the continental shelf mainly produce oil, and the southern basins located in the continental slope are gas producing basins. The Huizhou Sag (HZS), located in the north of the PRMB, is a typical rift basin during the Cenozoic. The recent explorations show that about 64% of petroleum reserves in the PRMB were found in intradepression highs on both northern and southern sides of the HZS [1]. In the 1990s, the petroleum exploration is mainly focused on the Oligocene postrift Zhuhai transitional formation (Fm) and overlying strata. Recently, there were more discoveries found in the Eocene syn-rift Wenchang and Enping Fm. Commercial oil flow was obtained in the Enping Fm exampled by well 254, and oil was found in the Wenchang Fm exampled by well 254 and well 81. In 2011, test results of the well 257 revealed oil in the Eocene tight sandstone reservoir with more than 4000 m depth in the HZS, and the oil flow of well 257 is up to 173 m^3 per day during production testing stage [2]. Three years later, tight oil was discovered in the LF13 fractured anticlinal structure belt in the Huilu area, and the oil flow of well 141 and well 81 is up to 210 m^3 per day during production testing stage [3]. The geological reserves of the new tight sandstone oil discovery are more than 9.6×10^7 m^3 in the well 257, well 144, and well 81 (according to the reserves report

of Shenzhen Company of CNOOC China Ltd.). The Eocene Wenchang and Enping Fm, developed in the lacustrine and swamp environment during the midcontinental rift stage, are generally considered to be two main sets of source rocks in the PRMB; the new discoveries not only indicated the huge hydrocarbon potential of the deep Eocene strata but also brought the new question about the petroleum migration of the Eocene source rocks in the HZS.

The driving forces for secondary petroleum migration are buoyancy and groundwater flow, and the restraining force is capillary pressure, which increases with decreasing pore-throat size, increasing interfacial tension and wettability [4–7]. However, the nature of petroleum migration pathway is still controversial. Some researchers [7–26] believed that the petroleum fluids migration is mainly driven by structural morphology, and modeling of petroleum fluids migration pathways can be a powerful tool to reduce exploration risk. Others [27–31] propose that petroleum fluids tend to pass through a high-permeable, thin sandstone bed than through a low-permeable and thick sandstone bed, controlled by the heterogeneity of the porosity and permeability of the carrier beds.

Because of incomplete geological data and few drilling wells, the mechanism of secondary hydrocarbon fluids migration in the PRMB is still unclear. Long et al. [32] believed that hydrocarbon migration was mainly controlled by the heterogeneity of carrier beds, while Shi (2013) concluded that structural morphology in the HZS was the primary control of petroleum migration pathway based on 3D computer modeling. The migration process and dominant pathway in the HZS are still poorly understood. In this paper, four wells and two regional sections are selected to analyze the process of hydrocarbon generation, fluids migration, and accumulation in the HZS of the PRMB.

2. Geological Setting

2.1. Tectonic Evolution and Sedimentary Character. The PRMB is located in the northern continental margin of the SCS, which covered an area of approximately 1.7×10^5 km^2. It consists of four depression zones, including the Zhu-I Depression, the Zhu-II Depression, the Zhu-III Depression, and the Chaoshan Depression, and three uplift zones including the North Uplift Zone, the Central Uplift Zone, and the Southern Uplift Zone (Figure 1(a)). The Zhu-I Depression has typical double-layer geologic structure of rift overlain by sag and was controlled by a series of major boundary faults [33]. The HZS is located in the central part of the Zhu-I Depression and characterized by half grabens or strongly asymmetric grabens (Figure 1 profile AA′ and profile BB′). The geological evolution of the PRMB is significantly influenced by the Philippine Sea plate, the Eurasian plate, and the Indo-Australian plate [34–36]. The HZS mainly has experienced three tectonic events during the Cenozoic: the Paleogene continental rift stage, the Miocene passive continental margin stage (postrift stage), and the Late Miocene-Quaternary Neotectonic stage (Figure 2). During the continental rift stage, the HZS developed the Paleocene Shenhu Fm, the Eocene Wenchang, Enping Fm, and the Oligocene Zhuhai Fm. The Eocene Wenchang Fm, the most important source rock, consists of dark lacustrine mudstone with gray fluvial sandstone and coal interbedded. The Eocene Enping Fm, minor source rock, is mainly composed of lacustrine-swamp mudstone, coal bed, and fluvial sandstone. The Oligocene transitional Zhuhai Fm is composed of light gray delta-littoral siltstone, which is the major reservoir in the HZS. During the passive continental margin stage (postrift stage), the HZS developed the Miocene Zhujiang and Hanjiang Fm. The Miocene formations of Zhujiang and Hanjiang consist mainly of littoral siltstone, neritic mudstone, marine mudstone, and carbonate. The widespread and muddy upper Zhujiang Fm acts as a regional cap rock. The Miocene Yuehai, Pliocene Wanshan, and the Quaternary Fm were deposited in a marine environment during Neotectonic stage. From the Palaeocene to the Neogene, there are three intervals of combinations of oil source rock, reservoir, and cap rock (Figure 2).

Due to regional extensional stresses, the HZS was a lacustrine basin during the sedimentary period of the Eocene Wenchang Fm. The provenance is mainly from the northwest and northeast direction and shoreline-shallow lacustrine and deep lacustrine facies developed in the Huixi half-graben, Huibei half-graben, Huizhong low-uplift, Huinan half-graben, and Huilu low-uplift. Under the regional extensional environment, high quality lacustrine source rocks were widely developed during the sedimentary period of the Wenchang Fm (Figure 3(a)). After that, the ancient lake basin shrank gradually during the sedimentary period of the Eocene Enping Fm, and a large amount of fluvial deposits came from the southwest, northwest, and northeast direction. The shoreline-shallow lacustrine mudstone and swamp coal-bearing strata developed in the Huixi half-graben, Huibei half-graben, and Huinan half-graben during the sedimentary period of the transgression systems tract of the Enping Fm (Figure 3(b)), and the fluvial-delta developed in the most areas during the sedimentary period of the highstand systems tract of the Enping Fm (Figure 3(c)).

2.2. Source Rock

2.2.1. Distribution of Source Rock. The lowstand and highstand systems tracts of the Wenchang Fm developed in the local areas, while the transgression systems tracts of the Wenchang Fm were deposited over a wide area in the HZS (Figure 3(a)). During the extensional rifting stage, shoreline-shallow lacustrine and deep lacustrine mudstones were formed. The thickness of lacustrine mudstone ranges from 200 m to 1000 m, and more than 750 m source rocks developed in the Huixi half-graben. The percentage of deep lacustrine mudstone in the well 132 reaches up to 82.5%, which is much more than that of shoreline-shallow lacustrine mudstone in the other wells (Table 1).

The lowstand systems tract of the Enping Fm developed in the limited area and mainly consists of fluvial-delta facies with lower percentage of source rocks. The transgression and highstand systems tracts of the Enping Fm are widely distributed in the HZS (Figures 3(b) and 3(c)). The transgression systems tract of the Enping Fm mainly consists of shoreline-shallow lacustrine mudstone and swamp

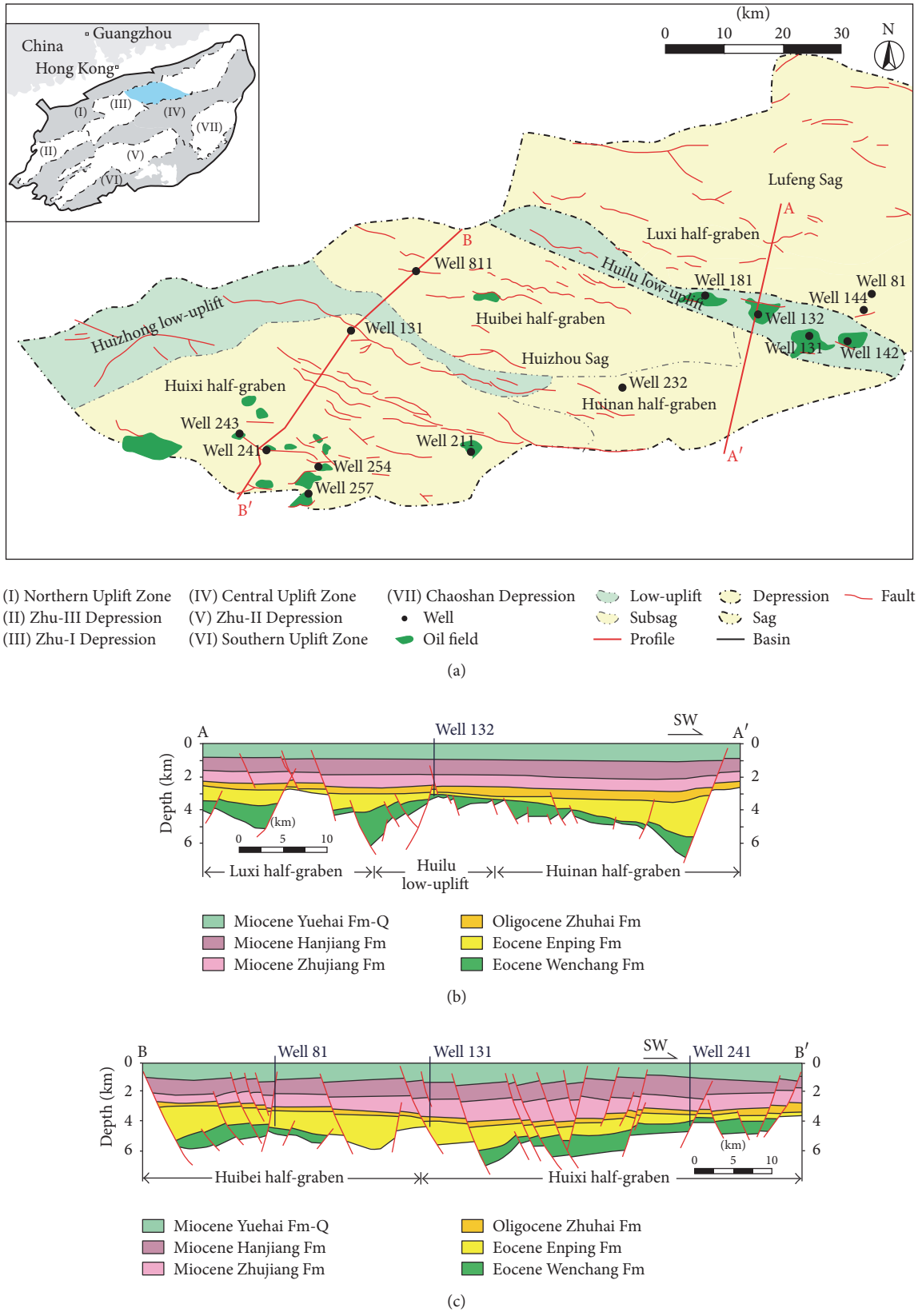

Figure 1: Regional location of the Huizhou Sag (a) and two geological profiles cross the Huilu low-uplift (b) and Huixi half-graben (c).

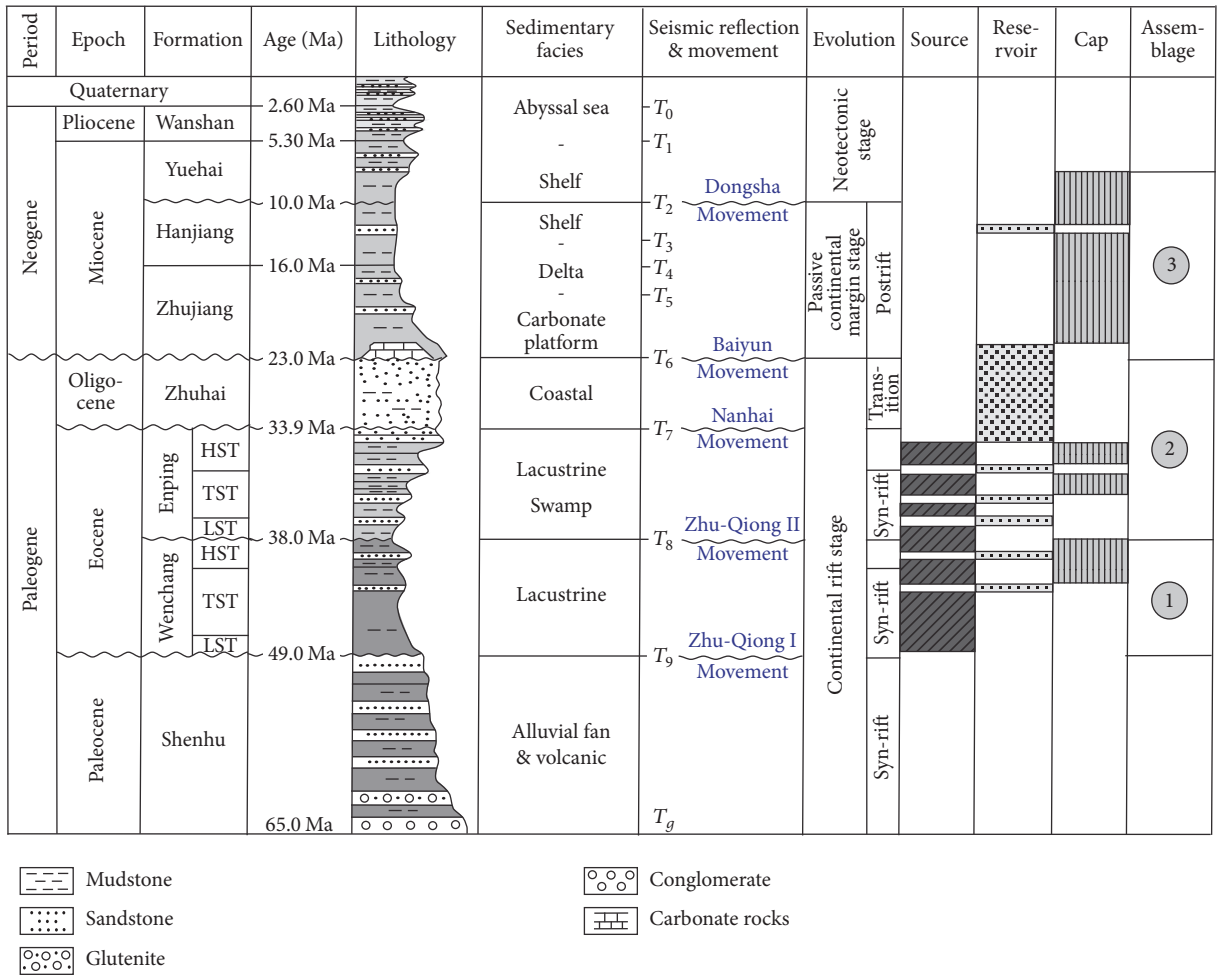

Figure 2: Simplified lithostratigraphy and source-reservoir-cap assemblage of the Huizhou Sag. See Figure 1 for the location of the Huizhou Sag (lithostratigraphic sequence modified from [37]). (LST: lowstand systems tract; TST: transgression systems tract; HTS: highstand systems tract.)

carbonaceous mudstone. The highstand systems tract of the Enping Fm mainly consists of shoreline-shallow lacustrine mudstone, swamp carbonaceous mudstone, and fluvial-delta mudstone. The percentage of mudstone in the Enping Fm is generally from 15%~40% (Table 1).

2.2.2. Kerogen Type. The composition and structure of kerogen depend on the origin of the organic matter from which it has evolved, as well as its degree of thermal evolution. In this study, total organic carbon (TOC) content was measured by using a LECO CS-400 analyzer, and Rock-Eval pyrolysis and organic petrology were used to identify the kerogen type of organic matter. Rock-Eval pyrolysis was performed by using a Rock-Eval II instrument. All the samples were heated to 600°C in a helium atmosphere to obtain the primary parameters, such as hydrocarbon generation (S_1) at a low temperature peak within a range of 150~300°C, hydrocarbon generation (S_2) at a high temperature peak in the range of 420~550°C, carbon dioxide (S_3), and the temperature at maximum rate of hydrocarbons generation (T_{max}) [39]. Because the oxygen index was not measured by Rock-Eval II instrument, the cross-plot of HI versus T_{max} was used to divide the kerogen type. According the pyrolysis experimental data of some wells in the HZS, the kerogen of the Wenchang source rock is mainly Type-II_1 and Type-I, and Enping source rocks are generally composed of Type-II_1 and Type-II_2 kerogen (Figure 4).

Organic petrography of the Eocene source rocks was also applied to characterize and identify the various organic constituent. Microscopic examination of the Eocene source rocks from 6 wells in the HZS was performed under transmission light. Various types of organic materials were recognized (Figure 5(a)): woody organic matter (W), coaly organic matter (I), exinite (E), cutinite (C), algal organic matter, and amorphous organic matter (AOM). Microscopic examination shows that the kerogens in the Eocene Wenchang source rocks are mainly classified into three types (Figure 5(b)). Type-I is dominated by amorphous organic matter, for example, algae, which was formed in the deep lacustrine environment with high productivity. Type-II is dominated by mixed organic matter rich in hydrogen maceral exinite, and Type-III is dominated by woody vitrinite, which were

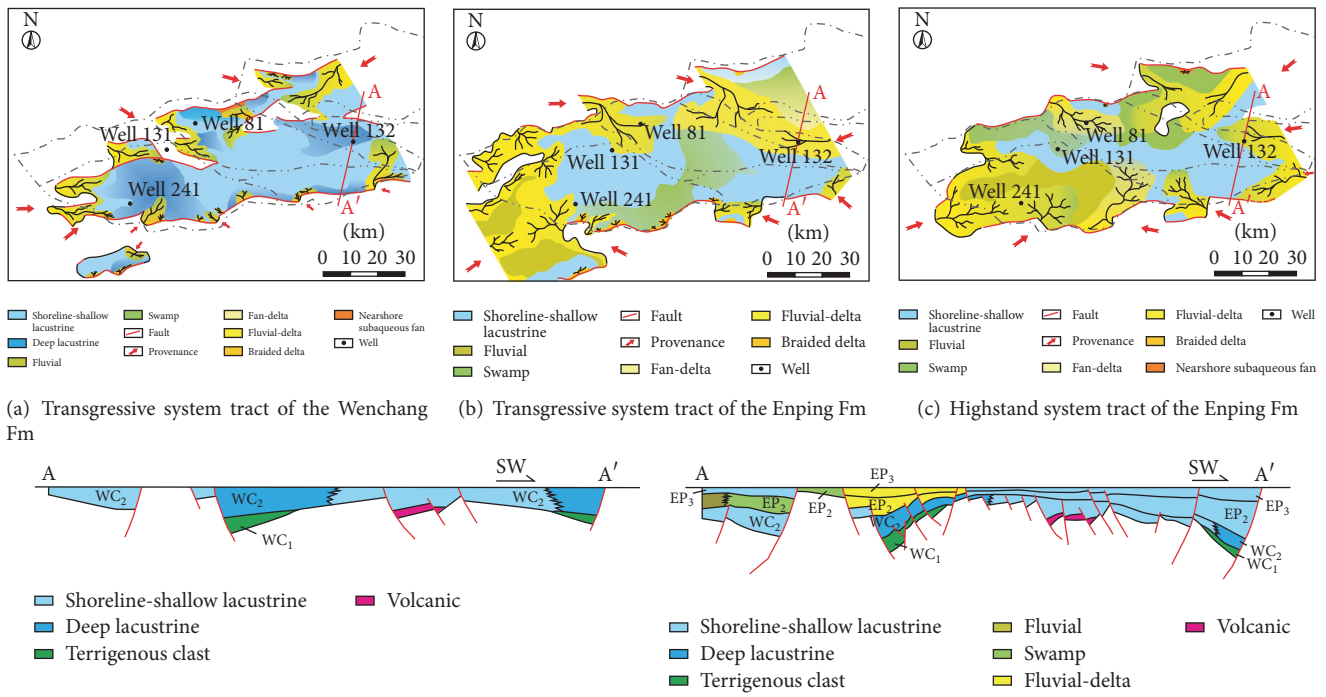

(a) Transgressive system tract of the Wenchang Fm

(b) Transgressive system tract of the Enping Fm

(c) Highstand system tract of the Enping Fm

(d) The sedimentary period of Wenchang Formation

(e) The sedimentary period of Enping Formation

Figure 3: Distribution of the lacustrine facies of the Wenchang and Enping Fm in the Huizhou Sag.

Table 1: The percentage of argillaceous source rock in the Huizhou Sag (HZS).

Formation	Well	Systems tracts*	Depth (m)	Facies	Percentage (%)
Eocene Wenchang	132	TST	3140–3280	Deep lacustrine	82.5
	241	TST	3601–3776	Fluvial	15.3
	243	TST	4013.5–4124	Shore-shallow lacustrine	62.7
	211	TST	4228–4456	Shore-shallow lacustrine	41.1
Eocene Enping	211	HST	3646–3811.07	Fluvial-delta	7.7
		TST	3811.07–4228	Swamp	14.7
	243	TST	3445–4130	Shore-shallow lacustrine	31.1
	181	HST	2919.5–3128	Fluvial-delta	29.5
	142	HST	2836.5–3155	Shore-shallow lacustrine	29.9
		TST	3155–3551	Fluvial-delta	20.6
	131	HST	2820–3078.4	Shore-shallow lacustrine	22.8
		TST	3078.4–3193	Fluvial-delta	15.1
	232	HST	3734.85–3969.02	Fluvial-delta	30.4
		TST	3969.02–4520	Shore-shallow lacustrine	23.7
		TST	3128–3254	Fluvial-delta	13.4
	131	HST	3805–4339.07	Swamp	33.3
		TST	4339.07–4804	Shore-shallow lacustrine	18.8
	81	HST	3170.5–3485.77	Delta	36.5
		TST	3485.77–3810.8	Delta	24.1
		LST	3810.8–4583	Fluvial	13.2
	231	HST	3646–3953.12	Fluvial-delta	25.7
		TST	3953.12–4250	Shore-shallow lacustrine	15
	132	HST	2848–3060	Fluvial-delta	40.8
		TST	3060–3140.05	Fluvial-delta	16.7

*LST: lowstand systems tract; TST: transgression systems tract; HTS: highstand systems tract. *Note*. Lithology data came from core analysis and cuttings logging.

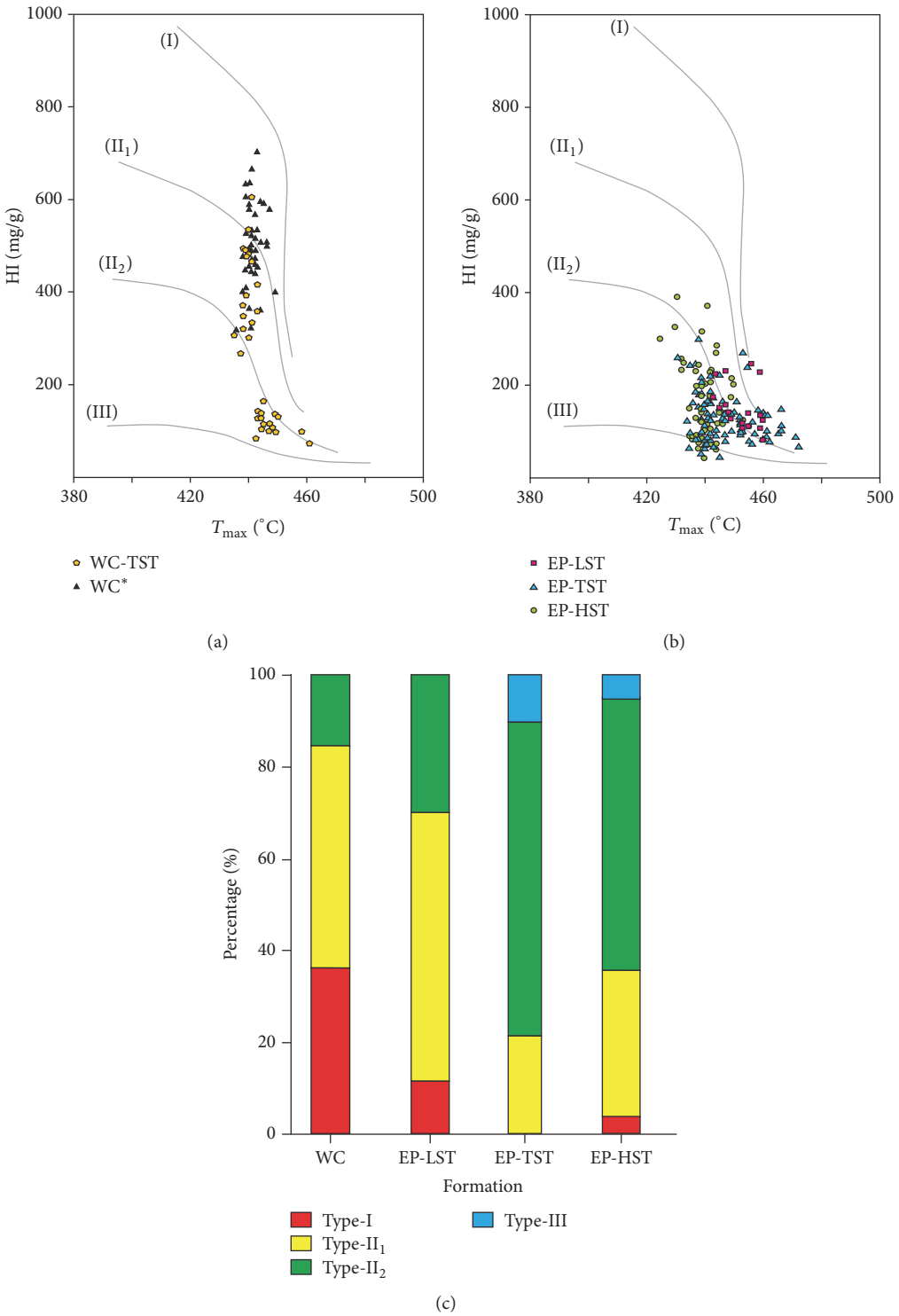

FIGURE 4: Kerogen types of the Eocene Wenchang and Enping source rocks in the Huizhou Sag (HI: hydrogen index, mg/g; T_{max}: the pyrolysis temperature at maximum amount of generated hydrocarbons, °C; WC: the Wenchang Formation; EP: the Enping Formation; LST: lowstand systems tract; TST: transgression systems tract; HTS: highstand systems tract; WC*: data from [38]).

mainly formed in shore-shallow lacustrine and fluvial environment. Microscopic examination of 6 wells shows that the organic matters of the Enping source rocks were mainly composed of terrestrial phytodetritus, formed in the oxygen-rich environment with high hydrodynamic force (Figure 5(b)). Organic maceral and submaceral characteristics of the Eocene source rocks in the HZS have been studied by means of composite optics of organic petrology by Zhu et al. [40].

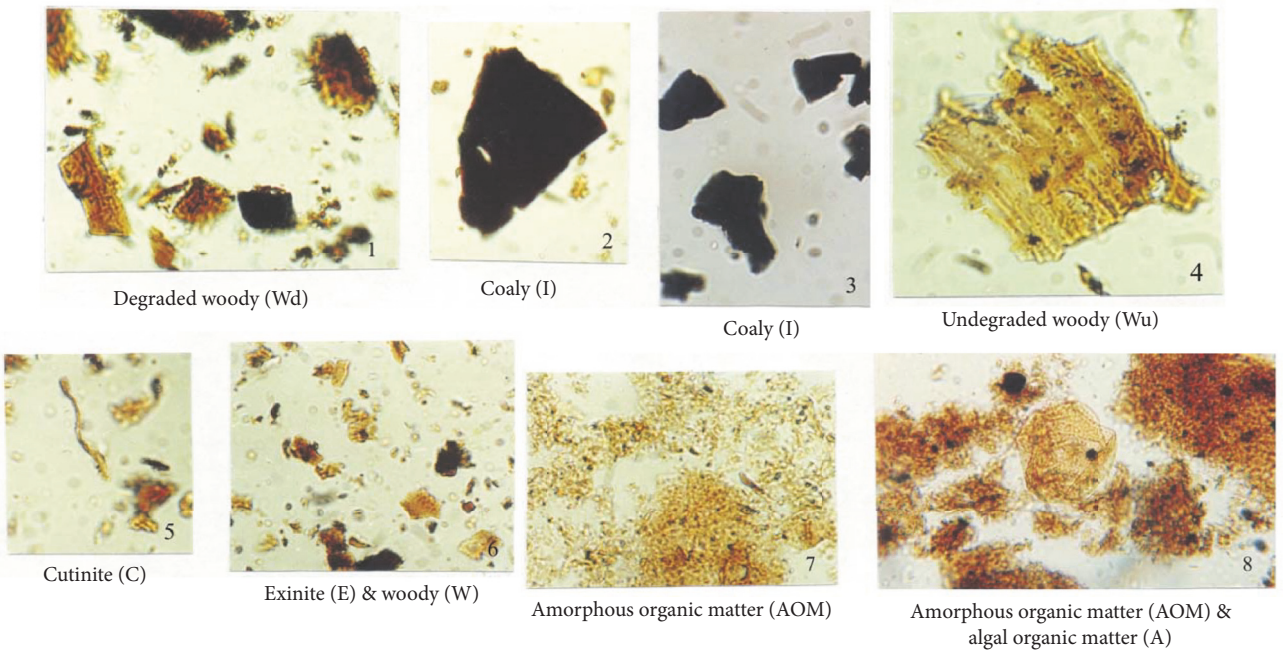

(a) Various organic matters observed under the microscope in the Wenchang and Enping source rocks

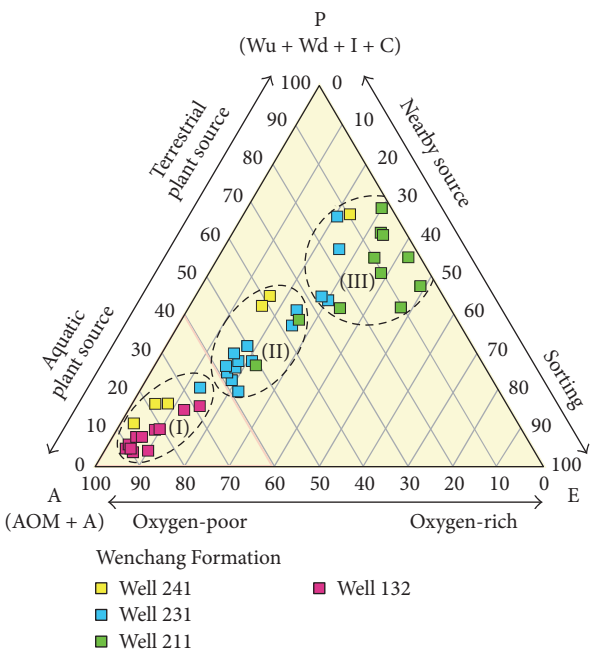

(b) Depositional environment of the Wenchang formation

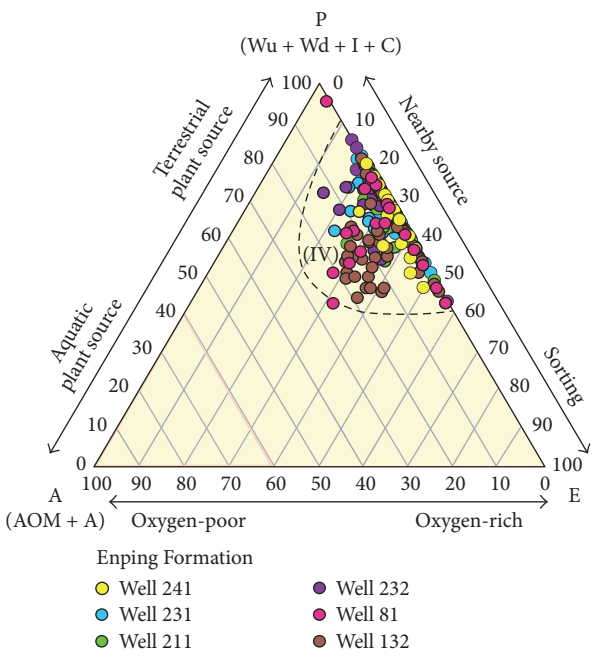

(c) Depositional environment of the Enping formation

Figure 5: Organic constituent (a) and P-A-E ternary diagrams of Wenchang source rocks (b) and Enping source rock (c) (P: higher terrestrial plant; A: amorphous organic matter and alginite; E: exinite and sporonin). Data according to the internal reports of Shenzhen Company of CNOOC China Ltd.

The results show that relatively abundant exinite rich in hydrogen results in oil-prone Types-I-II_1 of organic matter in deep lacustrine facies, while relatively abundant vitrinite results in gas and condensate-prone Types-III-II_2 of organic matter in shore-shallow lacustrine and swamp facies.

All these data indicated that the Eocene Wenchang source rocks are of Type-I/II/III mixed kerogens and the Eocene Enping source rocks are dominated by Type-II_2 kerogen with a small amount of Type-III. In the HZS, Type-III kerogen is generally poor to fair source rocks with limited hydrocarbon generating potential. Type-II_2 kerogen is fair to good source

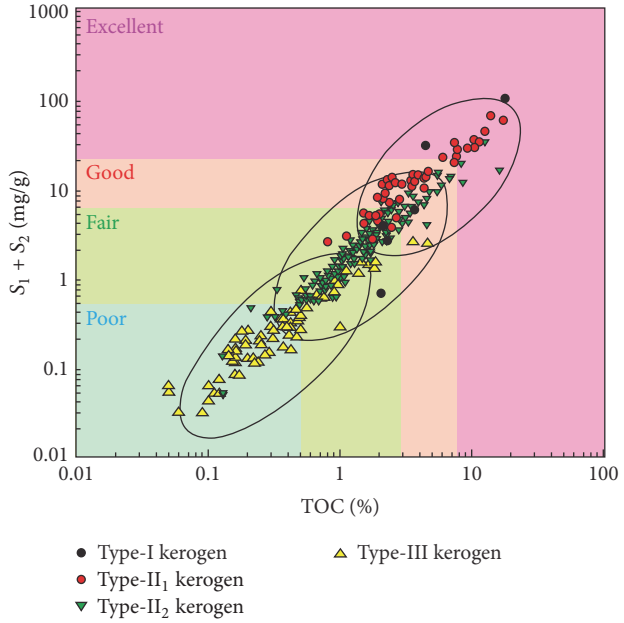

Figure 6: The relationship between the hydrocarbon generation potential (S_1 + S_2) and the total organic carbon (TOC) of the Eocene Wenchang and Enping source rocks developed during the continental rift stage in the Huizhou Sag.

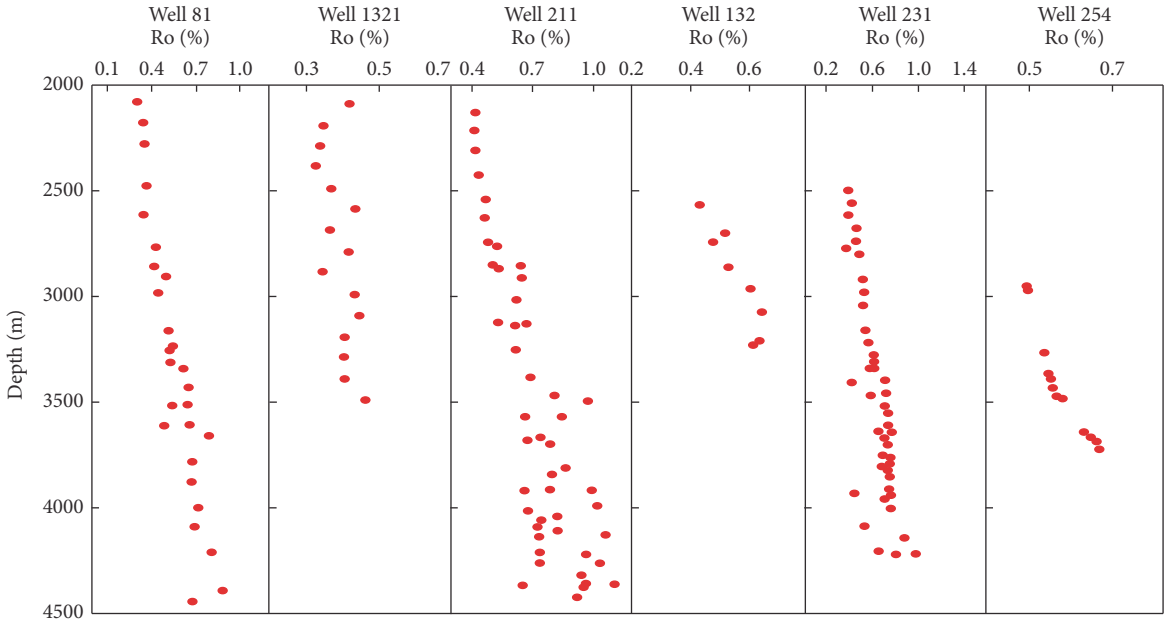

Figure 7: Measured vitrinite reflectance (Ro) of the Eocene source rocks in the Huizhou Sag.

rock, which contributed a lot to hydrocarbon generation, and Type-II$_1$ and Type-I kerogen are good to excellent source rocks, which made significant contribution to hydrocarbon generation in the HZS (Figure 6).

2.2.3. Maturity. Vitrinite reflectance (Ro) was measured by an oil immersion lens and a Leixa MPV Compact II reflected light microscope fitted with a microphotometer. Measured Ro values in six wells are primarily between 0.5% and 1.2%, indicating that the Eocene source rocks have entered the mature generation stage (Figure 7). T_{max} of the Eocene source rocks are mainly in range of 430°C to 460°C (Figure 8), which suggests that most source rocks in the HZS are sufficiently mature to have generated oil [41, 42]. Because samples from deeper sags are not available in the study area, these measured Ro data can not reflect the whole maturity of the Eocene source rocks. The theoretical maturity of deeper interval was calculated by using 1D burial and thermal history simulations. According to the previous research [3], the Eocene Wenchang source rock in the HZS is mature within

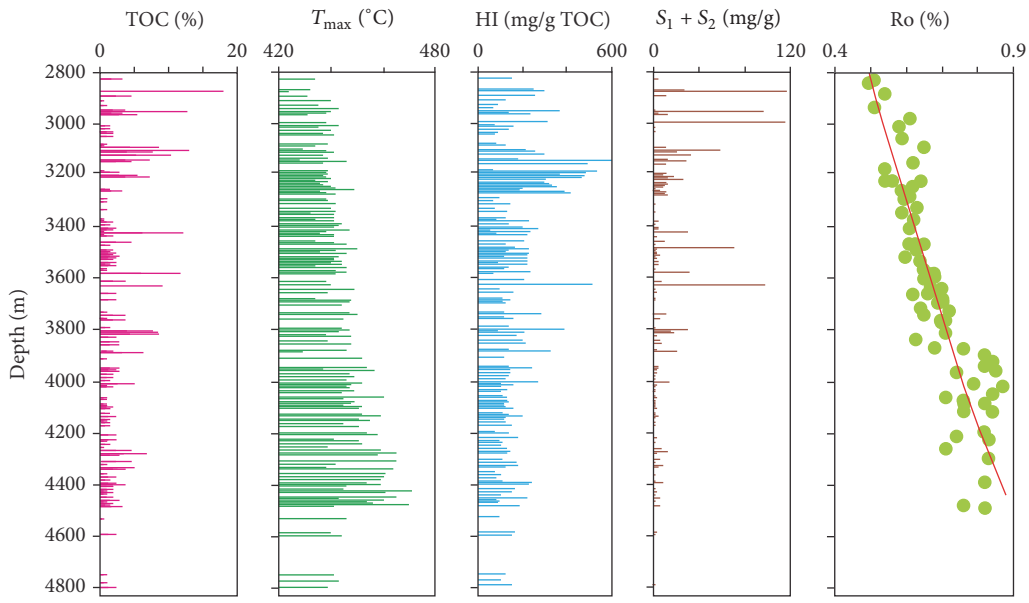

Figure 8: Measured geochemical parameters of the Eocene source rocks in the Huizhou Sag (HZS).

Ro range of 0.8%~1.8%, and the Enping source rock is in range of 0.6% to 1.4%.

2.2.4. Geochemical Characteristics. Table 2 lists the geochemistry characteristics of source rocks with different facies in the HZS. The Wenchang source rocks consist of various facies from swamp to deep lacustrine, with HI ranging from 83.5 mg/g·TOC to 613.1 mg/g·TOC. The TOC content of the Wenchang source rock ranges from 0.5% to 7.7%, with mean value of 2.0%. The highest TOC value of 7.7% is from the deep lacustrine dark mudstones of the well 132 (Figure 9). The Enping source rocks consist of swamp mudstone, swamp carbonaceous mudstone, and fluvial-delta mudstone. The fluvial-delta mudstone belongs to medium quality hydrocarbon source rocks, with TOC value ranging from 0.3% to 11.9%, of which hydrocarbon generation potentials ($S_1 + S_2$) ranged from 0.2 mg/g to 32.8 mg/g. The swamp-lacustrine mudstone belongs to medium-high quality hydrocarbon source rocks, with TOC value ranging from 0.6% to 6.9%, of which hydrocarbon generation potentials ($S_1 + S_2$) ranged from 0.6 mg/g to 27.1 mg/g. Because of the limited number and distribution of the source rock samples, the lateral variation of TOC in deeper undrilled part of the HZS was predicted by using the logging-seismic prediction technology. The relationship between measured TOC and well-logging values of sonic transit time, natural gamma, resistivity, density, and neutron was established to obtain the prediction models (Figure 9).

The ratio of pristane (Pr) and phytane (Ph) value is 6.35 in the Wenchang source rocks from well 243 with low content of 4-methyl sterane (Figure 10), which means that the source rocks were formed in a shallow water environment. The ratio of Pr/Ph value is 2.70 in the Wenchang source rocks from well 132 with high content of 4-methyl sterane, which indicates that the source rock is originated from lacustrine with algal input ([43, 44], Fu and Zhu, 2007). The ratio of Pr/Ph values is more than 6 in the Enping source rocks. The 4-methyl sterane content is low and the content of C_{29} sterane is relatively higher than the levels of C_{27} sterane and C_{28} sterane (Figure 10), which indicates that the Enping Fm developed in the environment containing both algal and land plant material ([43, 44], Fu and Zhu 2007).

2.3. Reservoir and Caprock. The Eocene sandstone and andesite of Wenchang Fm reservoir are the main reservoir [46]. Percentage of sandstone in the Wenchang Fm is 4.86% and 37.34%, respectively. Porosities of the Eocene Wenchang Fm from well 254 range from 4.9% to 25.3% (Figure 11(a)). The Enping reservoir is fluvial sandstone, with sandstone content of single well ranging from 24.13% to 71.19%. Porosities of the Enping Fm range from 9.0% to 20.0%, and permeabilities of the Enping Fm range from 0.1 to 28.4 mD (Figure 11(a)). Porosities of the Oligocene Zhuhai Fm range from 4.6% to 15.2% with average value of 9.0%, and permeabilities range from 0.004 mD to 223.0 mD. The sandstones of the Zhujiang Fm show considerable variation in porosity and permeability, with the measured porosities ranging from 5% to over 30% (Figure 11(b)) and the measured permeabilities ranging from 0.1 to over 1000 mD (Figure 11(c)). The average porosity and permeability of the upper Zhujiang Fm are 17.6% and 750 mD, respectively, and the average porosity and permeability of the lower Zhujiang Fm are 18.7% and 587 mD, respectively [47]. Overall, the Wenchang and Zhujiang Fm are strongly heterogeneous.

The Hanjiang, Zhujiang, and Wenchang Fm are the three regional seals in the HZS, which are characterized by wide distribution and thick cumulative thickness (Table 3). The lower Zhujiang Fm together with Enping Fm is the regional seals and Zhuhai Fm acted as the local seal.

Table 2: The characteristics of source rocks with different facies of the Eocene Wenchang and Enping Formation in the Huizhou Sag (HZS).

Well	Formation	Facies	TOC (%)	$S_1 + S_2$ (mg/g)	HI (mg·g^{-1})	Ro (%)
241	WC-TST	Shore-shallow lacustrine	0.94 (2)	1.29 (2)	119.5 (2)	/
211	WC-TST	Shore-shallow lacustrine	1.01 (2)	1.16 (2)	83.5 (2)	/
	EP-TST	Swamp	2.81 (1)	4.36 (1)	135 (1)	0.68~1.12 (23)
254	WC-TST	Lacustrine	0.73~2.89	2.40~11.26	43.1~334.30	0.67~0.74
			1.56 (12)	4.84 (11)	153.33 (12)	(10)
		Delta front	0.49~3.06	2.92~10.82	97.80~301.20	0.75~0.78
			1.44 (16)	4.49 (16)	173.09 (16)	(4)
132	WC-TST	Deep lacustrine	1.94~7.68	0.78~28.52	269.20~613.10	0.50~0.55
			3.24 (12)	12.77 (12)	430.31 (12)	(6)
	EP-HST	Delta plain	0.82~10.42	1.05~32.83	89.30~300.20	0.41~0.56
			4.72 (7)	10.86 (7)	187.27 (7)	(14)
243	WC-TST	Shore-shallow lacustrine	1.52~3.45	2.03~4.14	103.10~136.70	0.79~1.10
			2.15 (8)	2.86 (8)	124.15 (8)	(5)
	EP-HST	Fluvial	1.26~8.47	1.17~18.14	47.0~209.80	0.57~0.86
			3.10 (12)	5.38 (13)	124.72 (13)	(15)
142	EP-HST	Shore-shallow lacustrine	0.55~3.52	0.62~27.09	64.60~371.20	/
			1.80 (7)	4.84 (8)	134.84 (9)	
	EP-TST	Fluvial	0.30~7.26	0.24~18.42	56.70~248.30	/
			2.27 (19)	3.79 (19)	122.17 (19)	
232	EP-HST	Delta front	0.96~3.75	1.24~11.29	71.0~282.5	0.64~0.75
			2.01 (9)	4.29 (9)	139.73 (9)	(4)
	EP-TST	Delta plain	0.84~4.84	0.74~14.50	30.3~263.1	0.75~0.79
			1.53 (15)	2.71 (15)	95.29 (15)	(3)
		Shore-shallow lacustrine	0.84~6.91	0.81~12.32	43.0~115.80	0.87~0.94
			2.14 (16)	2.90 (16)	53.29 (16)	(6)
131	EP-HST	Delta plain	0.63~5.98	0.84~21.67	65.0~312.40	0.71~0.96
			2.19 (9)	5.66 (9)	148.47 (9)	(6)
	EP-TST	Delta plain	0.47~2.95	0.66~8.58	51.30~218.80	0.76
			1.85 (7)	4.04 (7)	135.99 (7)	(1)
		Fluvial	0.55~1.53	1.33~2.72	63.60~113.50	/
			0.92 (3)	1.79 (3)	88.23 (3)	
81	EP-HST	Delta	1.06~11.85	3.10~31.0	117.0~260.20	0.53~0.67
			3.23 (8)	8.73 (8)	201.21 (8)	(6)
	EP-TST	Fluvial-delta	0.93~4.32	1.90~10.10	87.10~307.70	0.56~0.81
			1.91 (9)	5.02 (9)	180.45 (9)	(7)
	EP-LST	Fluvial	0.66~11.43	1.80~31.30	40.10~209.40	0.62~0.91
			2.56 (13)	5.37 (13)	101.55 (13)	(7)

TOC: total organic carbon content, %; $S_1 + S_2$: hydrocarbon generation potential, mg/g; HI: hydrogen index, mg/g; Ro: measured vitrinite reflectance, %. WC: the Wenchang Formation; EP: the Enping Formation; LST: lowstand systems tract; TST: transgression systems tract; HTS: highstand systems tract. *Note*. The data are presented as in the following example: 0.55~3.52 shows minimum~maximum; 1.80 (7) shows mean (sample number). The value of measured vitrinite reflectance varies with depth, so Ro data are present without average values.

3. Modeling Method and Parameters

3.1. Method. In this study, 1D and 2D models were reconstructed using the petroleum modeling software BasinMod 2012. Four representative wells from the Huixi half-graben and the Huilu low-uplift (Figure 1(a)) were selected to perform 1D simulation by BasinMod 1D module in order to better understand the burial and thermal history in the rift and postrift setting and reveal the timing of hydrocarbon generation and expulsion. The calculated and calibrated results of 1D modeling were then input into 2D models [48]. As most oil fields are concentrated in the Huixi half-graben and the Huilu low-uplift, two seismic lines (Figure 1(a)) covering two areas with available measured data were selected to reconstruct the process of petroleum generation, fluid migration, and accumulation by BasinMod 2D module. With the available wells and seismic data, the hydrocarbon generation could be estimated quantitatively, while the process of

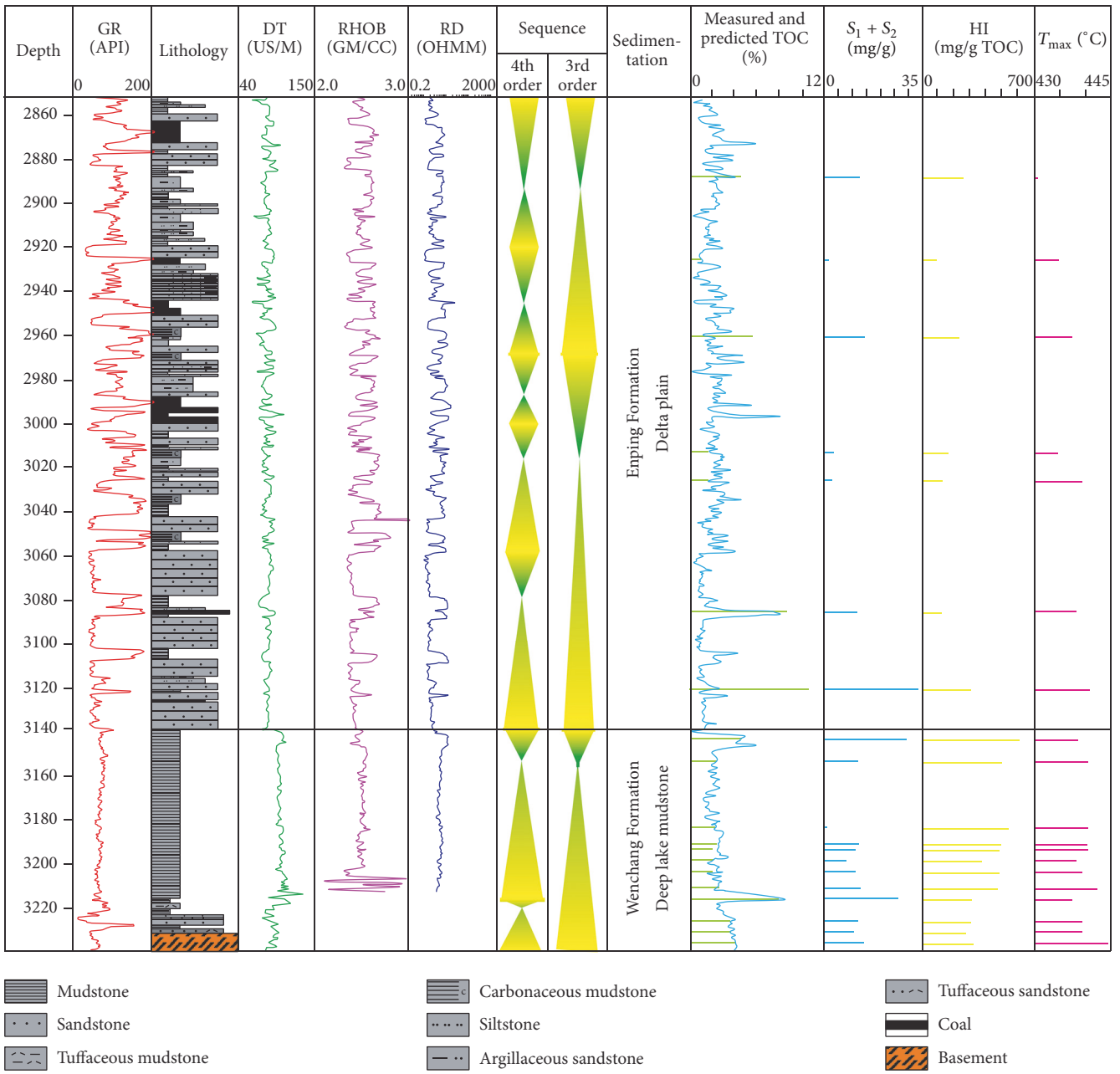

Figure 9: Well-logging and geochemistry parameters of well 132 in the Huizhou Sag (HZS). Measured TOC data are shown in green bar and the predicted TOC data using well-log curves calibrated by measured data are shown in blue curve.

Table 3: Parameters of mudstone seal in the Huizhou Sag [38].

Formation	Thickness (m)	Max thickness (m)	Average thickness of single layer (m)	Seal/stratum ratio (%)	Breakthrough pressure/Mpa
Hanjiang	46.0~700.0	13.0~91.0	4.3~34.0	18.0~87.0	0.2~1.5
Upper Zhujiang	72.0~638.0	34.0~121.0	2.0~52.0	27.6~86.0	0.4~30.0
Lower Zhujiang	16.0~120.0	7.0~41.0	3.0~16.0	8.5~76.0	1.0~30.0
Zhuhai	16.5~167.0	3.5~27.0	1.2~6.0	6.4~41.2	0.70~50.0
Enping	21.0~555.0	4.0~40.0	0.9~6.4	10.5~80.0	0.3~50.0
Wenchang	90.0~146.0	25.0~80.0	3.0~10.0	46.4~78.9	10.0~35.0

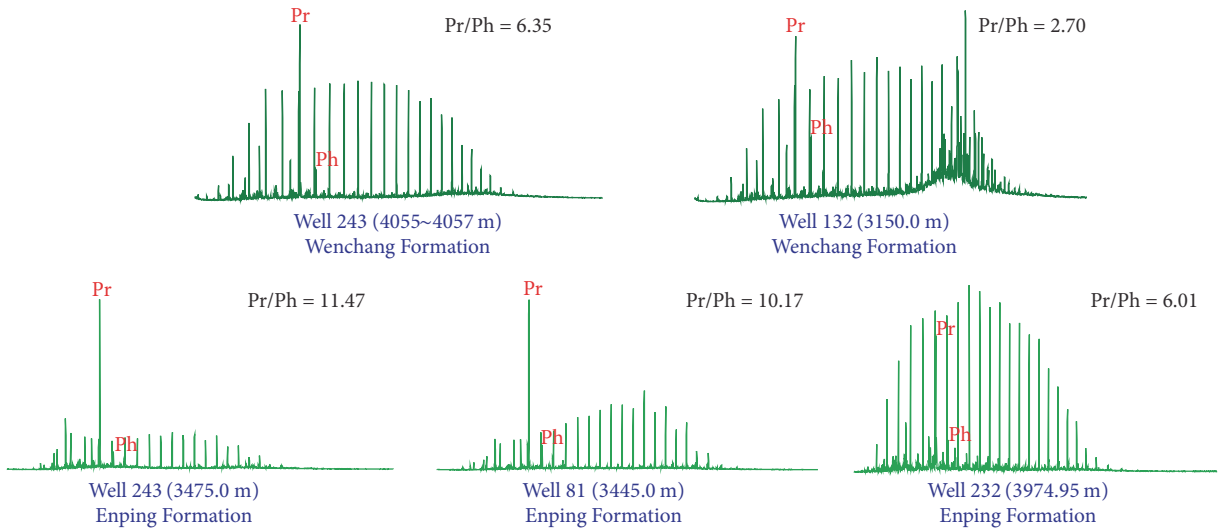

(a) The pristane/phytane (Pr/Ph) ratios of the source rocks in the Huizhou Sag (M/z = 85)

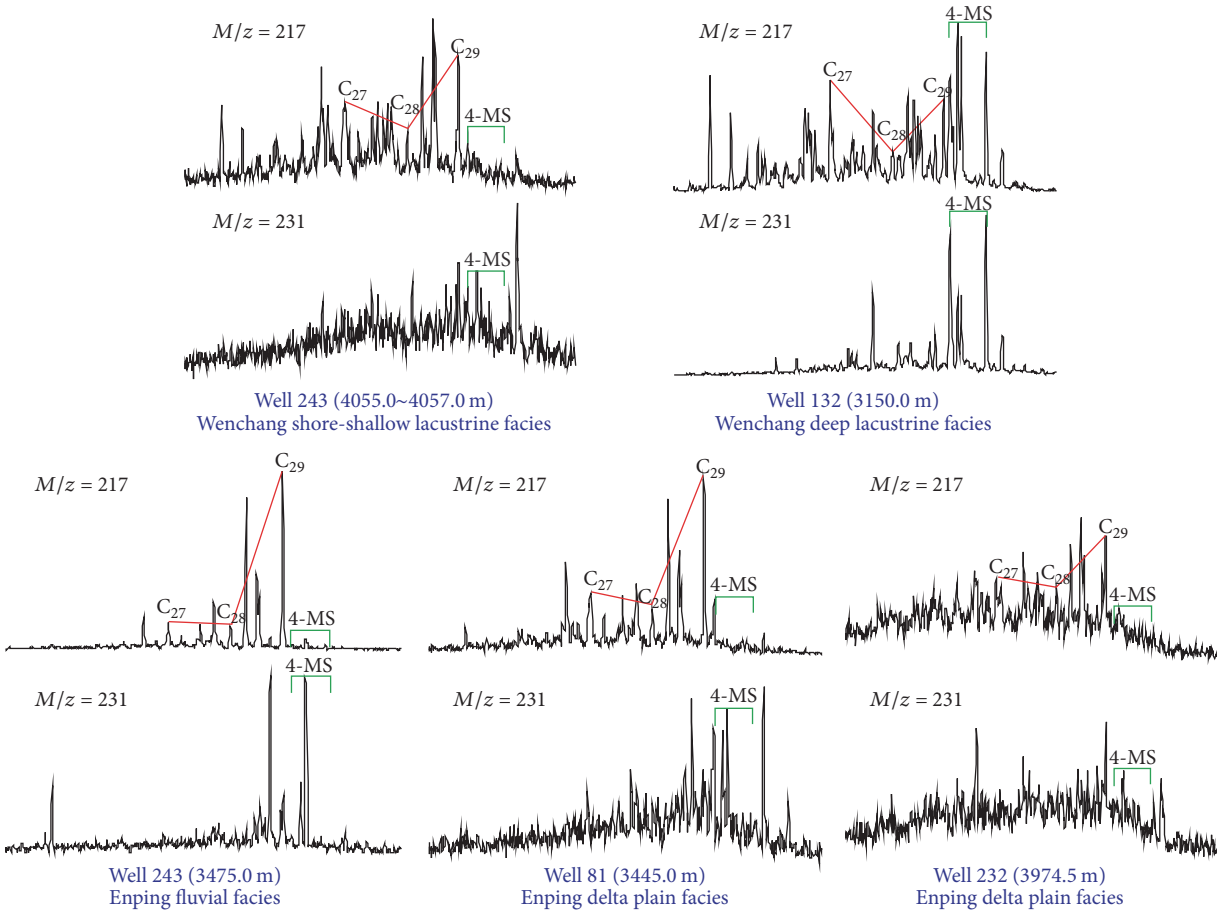

(b) Representative partial mass chromatograms (m/z = 217,231) of the saturate fractions for the Eocene source rocks in the Huizhou Sag (4-MS represents 4-methyl sterane; C27, C28, and C29 represent C_{27} sterane 20R, C_{28} sterane 20R, and C_{29} sterane 20R, resp.).

Figure 10: Representative gas chromatography and partial mass chromatograms of saturates in the Huizhou Sag (HZS) [45].

migration and accumulation has been studied qualitatively to semiquantitatively during the rift and postrift stage. The 3D modeling of fluid flow will not be discussed in this paper due to commercial confidentiality.

The reconstruction of burial history was based on geological information, tectonostratigraphic history of the region, and drilling and seismic data. Exponential compaction correlation method [49] was employed in this paper to reconstruct

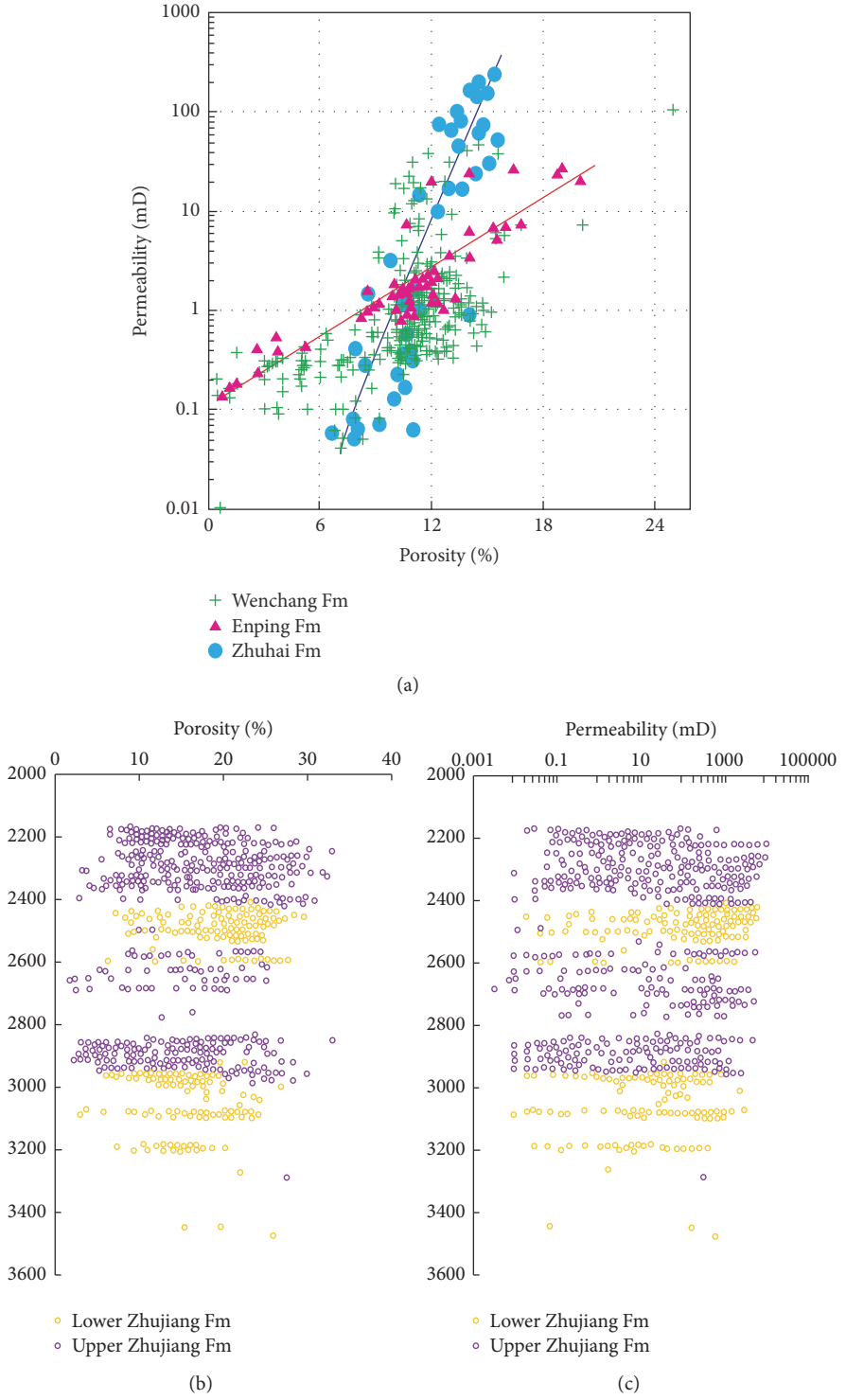

FIGURE 11: Porosity and permeability of the Paleogene (a) and Miocene (b, c) reservoir in the Huizhou Sag (physical properties of the Cenozoic reservoir modified after Peng et al. [3, 47]).

the burial history of strata in the HZS. Porosity is calculated by the following equation:

$$\Phi = \Phi_0 \exp^{-Kz}, \quad (1)$$

where Φ is porosity (%), Φ_0 is the initial surface porosity (%), K is the compaction factor for each lithology (cm^{-1}), and z is depth (m). Parameters for various lithologies under normal pressure are shown in Table 4.

Table 4: Parameters for various lithologies in exponential relationship.

Lithology	Φ_0	K
Shale	0.63	0.51×10^{-5}
Sand	0.49	0.27×10^{-5}
Chalk	0.70	0.71×10^{-5}
Shaly sand	0.56	0.39×10^{-5}

Permeability was calculated by the following equation [50]:

$$K = \frac{0.2\Phi^3}{S_0^2(1-\Phi)^2}, \quad \Phi \geq 10\%$$
$$K = \frac{20\Phi^5}{S_0^2(1-\Phi)^2}, \quad \Phi < 10\%, \tag{2}$$

where K is permeability (mD), Φ is porosity (%), and S_0 is the specific surface area of the rock (m^2).

Maturity and hydrocarbon generation were simulated by using the LLNL EASY% Ro model [51, 52], which was calibrated by the measured vitrinite reflectance (Ro%) and bottom hole temperature data. Expulsion calculation followed the saturation expulsion method [53] which assumed that the hydrocarbon will begin to be expelled from the source rocks when saturation of hydrocarbons reached a certain threshold related to the rock types and properties [54]. The irreducible water saturation was defined as 1.0.

Hydrocarbon migration was simulated by the transient migration model, which is based on the state equation, the mass conservation law, and the movement equation. The relative permeabilities of gas, oil, and water are calculated from the saturation-permeability relationship, and capillary pressure of gas and oil is calculated from saturation. Two main assumptions of migration in BasinMod are as follows: (1) There is no mass transfer between oil and gas phases during migration in one time step. (2) Migration of gas is much faster than that of oil and water, which occurs before the migration of water and oil. The migration of three-phase (oil, gas, and water) is accomplished by a two-step and two-fluid (gas-liquid and oil-water) migration calculation in BasinMod. The fluid flow equations ([55], Aziz & Settari, 1986, Freeze & Cherry, 1979) during the first migration step are written as follows:

$$\frac{\partial}{\partial x}\left[\Delta y \lambda X_g \left(\frac{\partial P_g}{\partial x} - \gamma_g \frac{\partial h}{\partial x}\right)\right] + \frac{\partial}{\partial z}\left[\Delta y \lambda Z_g \left(\frac{\partial P_g}{\partial z} - \gamma_g \frac{\partial h}{\partial z}\right)\right] = \Delta y \left[\frac{\partial}{\partial t}\left(\Phi \frac{S_g}{B_g}\right) + q_g\right]$$
$$\frac{\partial}{\partial x}\left[\Delta y \lambda X_l \left(\frac{\partial P_l}{\partial x} - \gamma_l \frac{\partial h}{\partial x}\right)\right] + \frac{\partial}{\partial z}\left[\Delta y \lambda Z_l \left(\frac{\partial P_l}{\partial z} - \gamma_l \frac{\partial h}{\partial z}\right)\right] = \Delta y \left[\frac{\partial}{\partial t}\left(\Phi \frac{S_l}{B_l}\right) + q_l\right] \tag{3, 4}$$
$$P_c = P_g - P_l \tag{5}$$
$$S_g + S_l = 1. \tag{6}$$

The fluid flow equations (Aziz & Settari, 1986, Freeze & Cherry, 1979) during the second migration step are written as follows:

$$\frac{\partial}{\partial x}\left[\Delta y \lambda X_o \left(\frac{\partial P_o}{\partial x} - \gamma_o \frac{\partial h}{\partial x}\right)\right] + \frac{\partial}{\partial z}\left[\Delta y \lambda Z_o \left(\frac{\partial P_o}{\partial z} - \gamma_o \frac{\partial h}{\partial z}\right)\right] = \Delta y \left[\frac{\partial}{\partial t}\left(\Phi \frac{S_o}{B_o}\right) + q_o\right]$$
$$\frac{\partial}{\partial x}\left[\Delta y \lambda X_w \left(\frac{\partial P_w}{\partial x} - \gamma_w \frac{\partial h}{\partial x}\right)\right] + \frac{\partial}{\partial z}\left[\Delta y \lambda Z_w \left(\frac{\partial P_w}{\partial z} - \gamma_w \frac{\partial h}{\partial z}\right)\right] = \Delta y \left[\frac{\partial}{\partial t}\left(\Phi \frac{S_w}{B_w}\right) + q_w\right] \tag{7}$$
$$P_c = P_o - P_w$$
$$S_o + S_w = 1.$$

The whole migration step was calculated with closed boundary (Γ_2):

$$q_l = \lambda_i \left(\nabla P_i - \gamma_i \nabla h\right) \quad n = 0,\ i = g, l, o, w \text{ on } \Gamma_2. \tag{8}$$

And initial condition is as follows:

$$\frac{dP_i}{dz} = \gamma_i \quad i = g, l, o, w \text{ on } \Gamma_2, \tag{9}$$

where $i = g, l, o, w$ (gas, liquid, oil, and water phases, resp.), Δy is the definition of thickness in y-direction, h is elevation (m, positive downwards), λX_i is x-direction transmissibility ($\lambda X_i = k_{xi}/\mu_i B_i$), λZ_i is z-direction transmissibility ($\lambda Z_i = k_{zi}/\mu_i B_i$), K_{xi} is the relative permeability of phase i in x-direction, K_{zi} is the relative permeability of phase i in z-direction, P_i is pressure of phase i (MPa), P_c is the capillary pressure (MPa), γ_i is the density in terms of pressure/distance ($\gamma_i = \rho_i g/g_c$), ρ_i is the density of phase i (kg/m^3), g is the gravitational acceleration (m/s^2), g_c is the conversion constant ($32.2\ lb_m/lb_f \cdot ft/sec^2$), S_i is the saturation of phase i (%), and B_i is the formation volume factors defined by

$$B_o = \frac{[V_i]_{\mathrm{RC}}}{[V_i]_{\mathrm{stc}}}, \tag{10}$$

Table 5: Lithology and petrophysical parameters of strata in the Huizhou Sag.

Formation	Percentage of pure lithology (%)			Density (g/cm^3)	Initial porosity	Thermal conductivity (W/m°C)
	Sandstone	Siltstone	Shale			
Wenchang	30.0	0	70.0	2.61	0.55	2.07
Yuehai	56.67	18.3	25.03	2.63	0.50	2.91
Hanjiang	45.99	33.47	20.54	2.62	0.51	2.71
Upper Zhujiang	30.0	0	70.0	2.62	0.55	2.07
Lower Zhujiang	70.0	0	30.0	2.63	0.49	3.19
Zhuhai	61.2	9.0	29.8	2.63	0.50	2.97
Enping	58.2	7.0	34.8	2.63	0.50	2.86
Wenchang	25.0	0	75.0	2.61	0.56	1.96

where $[V_i]_{RC}$ is the volume occupied by a fixed mass of component i ($i = g, l$) at the reservoir condition and $[V_i]_{stc}$ is the volume occupied by the same component i ($i = g, l$) at standard conditions.

Density of generated oil and gas is calculated by the hydrocarbon kinetics module. During the migration process, the density of fluids is calculated by pressure and temperature as follows:

$$\rho = \rho_{SC} \cdot \exp\left[\beta\left(P - 0.1\right) - \alpha\left(T - 25\right)\right], \tag{11}$$

where ρ_{SC} is the density at standard surface conditions (kg/m^3), α is constant (5×10^{-4} °C^{-1}), and β is constant (4.3×10^{-4} MPa^{-1}).

Density of water can be used as surface water density or a calculated water density under calculated temperature and pressure in the BasinMod software. The default value of surface water density is 1.3 gm/cm^3. The equation used for calculating water density considering temperature and pressure is written as follows:

$$\rho_{w=\rho_w^0 \cdot (1.0+\text{Pres.Term}-\text{Temp.Term})}, \tag{12}$$

where ρ_w is the calculated water density (kg/m^3), ρ_w^0 is the initial water density (kg/m^3), Pres.Term = $4.3 \times 10^{-10} \times (P - 1.013255 \times 10^5)$ (Pa), and Temp.Term is $5.0 \times 10^{-4} \times (T - 298.15)$ (K).

The viscosity of fluids for the modeling is obtained from an empirical formula fitted to viscosity versus temperature data as follows (after CRC Handbook of Chem. & Physics, 1986):

$$\mu = 10^n$$
$$n = \frac{1.3272 \cdot (20 - T) - 0.001053 \cdot (T - 20)^2}{T + 105}, \tag{13}$$

where T is temperature (°C) and μ is viscosity (Pa·s).

Fluid flow equations together with sediment compaction are written below. The measured pressure data were used in this study as calibration data.

$$\Phi = \frac{e}{1 + e} \tag{14}$$

$$e = e_{*A}\left(\frac{P_f}{P_{f*}}\right)^A \cdot (\text{Fraction } A) + \left[e_{*B} - B\left(P_f - P_{f*}\right)\right](\text{Fraction } B) \tag{15}$$

$$P_{\text{excess}} = P_{\text{overburden}} - \left(P_{\text{hydrostatic}} - P_{\text{frame}}\right), \tag{16}$$

where e is void ratio, e_{*A} is the initial void ratio of Fraction A, e_{*B} is the initial void ratio of Fraction B, P_f is frame, or matrix, pressure (Pa), P_{f*} is initial frame, or matrix, pressure (Pa), A is the exponential compaction factor, B is the linear compaction factor, and Fraction A is the portion of lithology which compacts exponentially, that is, all lithologies except sands. Fraction B is the portion of lithology which compacts linearly, that is, all sands.

3.2. Modeling Parameters

3.2.1. Formation Tops and Lithologies. The formation tops and lithologies were obtained from drilling results and seismic data. The lithology of each stratum (Table 5) was defined by mixing pure lithologies with specific petrophysical parameters and corrected according to the published work [3, 38, 56]. The functions "Facies Palette," "Thin Bed," and "Lenses and Mounds" were used to capture the laterally and vertically lithological variation and the heterogeneity of reservoir (Figure 12).

3.2.2. Tectonic Event. Several tectonic events have been recognized in the HZS (Figure 2). During the Paleogene continental rift stage, the Zhu-Qiong I (49.0 Ma) and Zhu-Qiong II Movement (38.0 Ma) not only formed the structural configuration of the HZS [43, 44, 57] but also developed regional unconformities (Figure 13(f)). In the early Oligocene, the Nanhai Movement (33.9 Ma) shifted the HZS from rifting

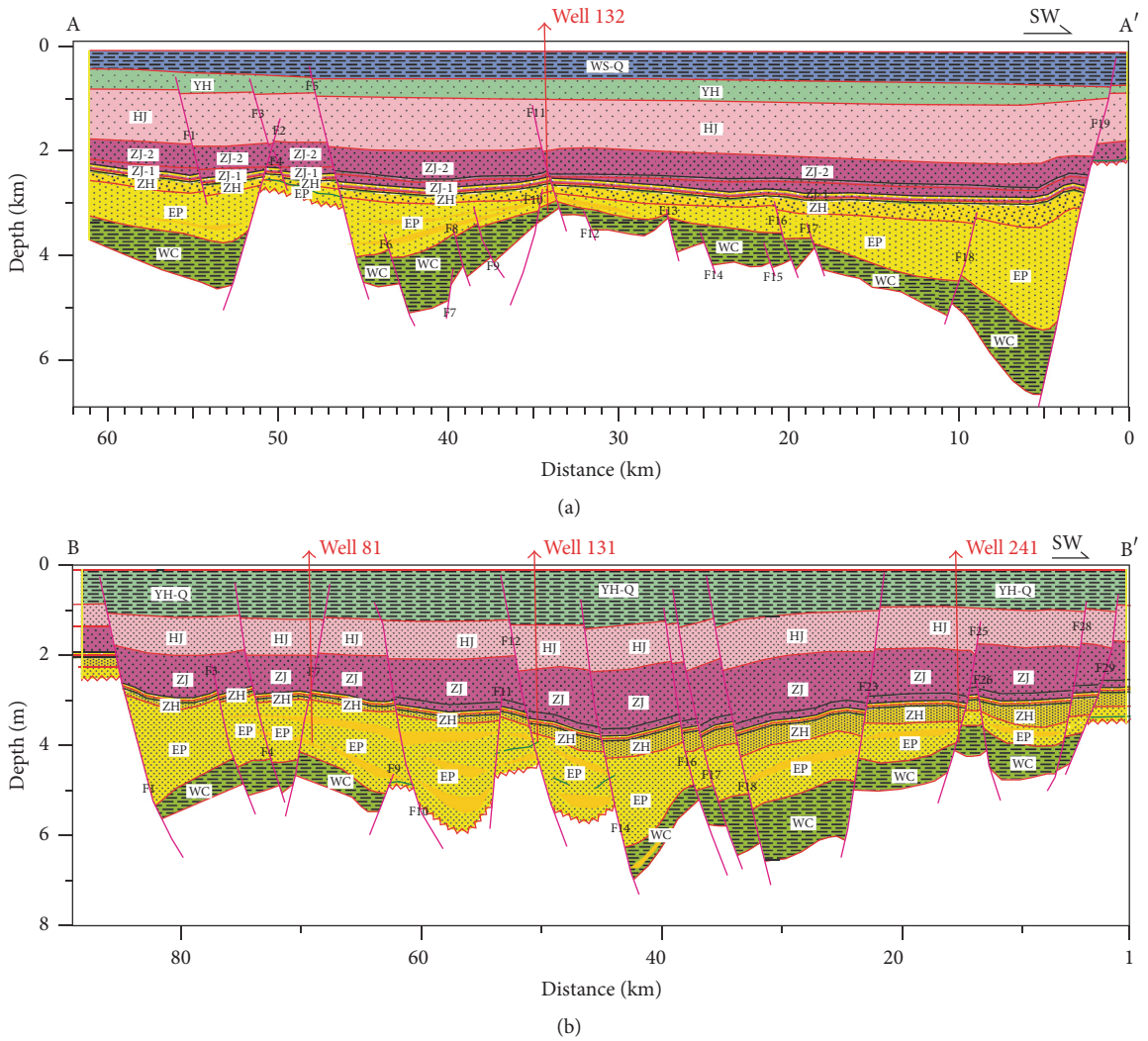

Figure 12: Two conceptual models with heterogeneous lithology in the Huizhou Sag (the locations of the profiles are shown in Figure 1). Formation names: WC = the Eocene Wenchang Formation; EP = the Eocene Enping Formation; ZH = the Oligocene Zhuhai Formation; ZJ = the Miocene Zhujiang Formation; HJ = the Miocene Hanjiang Formation; YH = the Miocene Yuehai Formation; WS-Q = the Pliocene Wanshan Formation to Quaternary; YH-Q = the Miocene Yuehai Formation to Quaternary.

to steady thermal subsidence (Figure 13(e)). These three movements developed most important unconformities in the HZS, which caused previous lacustrine source rocks to be eroded in the uplift area. The HZS entered the marine sedimentary environment after the Baiyun Movement (23.0 Ma), and fault activity decreased significantly (Figures 13(c) and 13(d)). During the Late Miocene-Quaternary Neotectonic stage, Dongsha Movement (10.0 Ma) led old faults to be reactivated and many new west-northwest-trending faults developed (Figure 13(b)). The most significant erosion events are related to the SCS opening process after the deposition of Eocene Enping Fm.

As regional tectonic events, the most significant unconformities formed at the end of the sedimentary period of the Wenchang and Enping Fm. As available measured Ro data is insufficient, the eroded thickness was estimated by extrapolation method of stratum trend (Figure 14). Erosion of the Wenchang Fm was mainly distributed in four areas, which are the Huixi and Huibei half-graben with erosion thickness of 600~1200 m, Huidong half-graben with erosion thickness of 500~1200 m, and Luxi half-graben with erosion thickness of 200~600 m [58]. Erosion of the Enping Fm was thinner than that of the Wenchang Fm, ranging from 100~400 m [58]. For the structure, only those faults with significant throw were included into the models in order to simplify the geology for saving the computation time.

3.2.3. Kinetic Models. Li et al. [60] suggested that the activation energy of the Wenchang dark mudstone primarily ranges from 46 to 63 kcal/mole, and their hydrocarbon generation potentials have a negatively skewed distribution. Jiang et al. [61] analyzed the chemical kinetic equations of the Enping dark mudstone and carbonaceous mudstone, which showed that dark mudstone has an activation energy of 49.5~64 kcal/mole with a normal distribution of the hydrocarbon generation potential, and carbonaceous mudstone has an

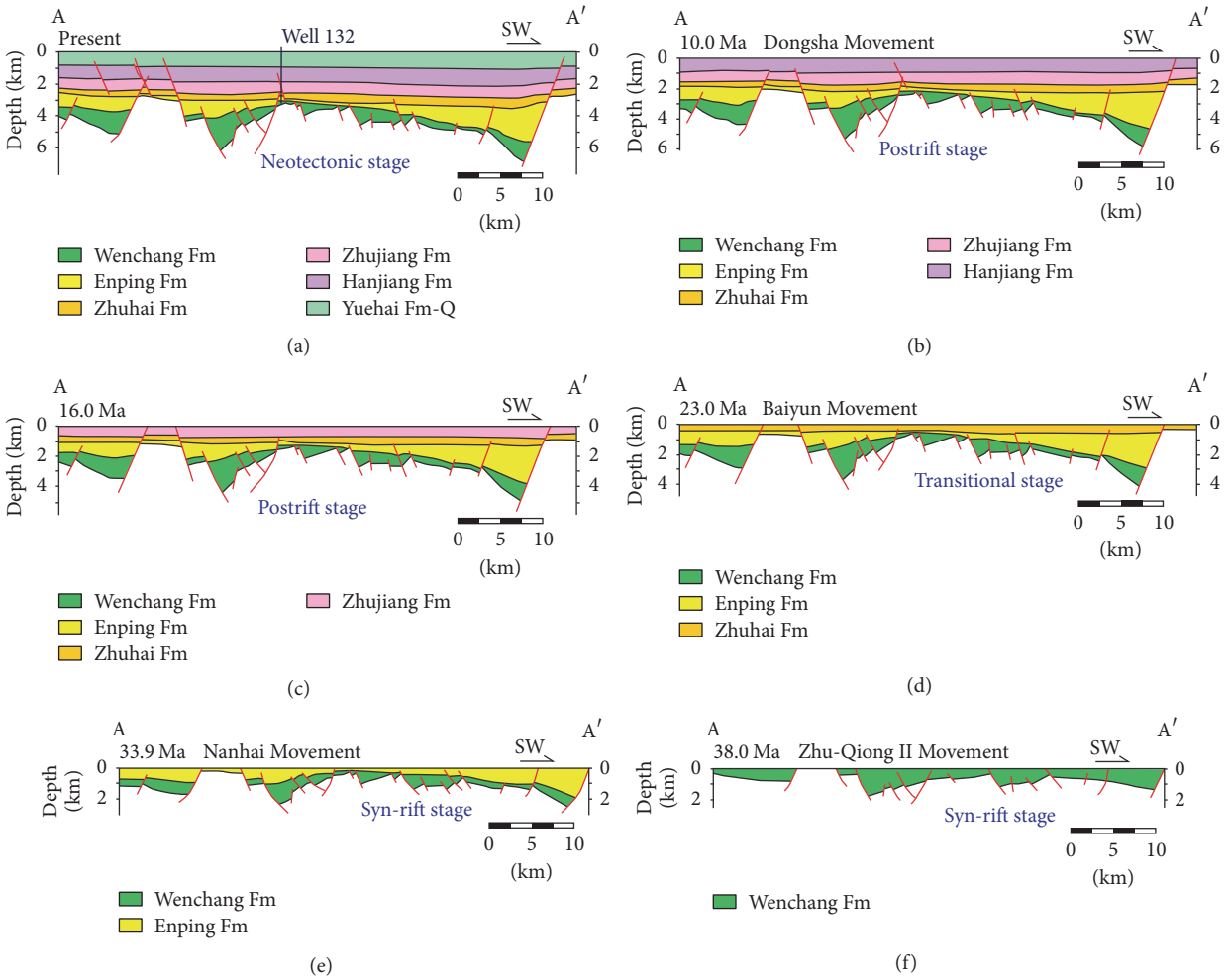

Figure 13: Tectonic evolution of the Huizhou Sag during the Paleogene rift stage and Neogene postrift stage (the locations of the profile AA′ is shown in Figure 1).

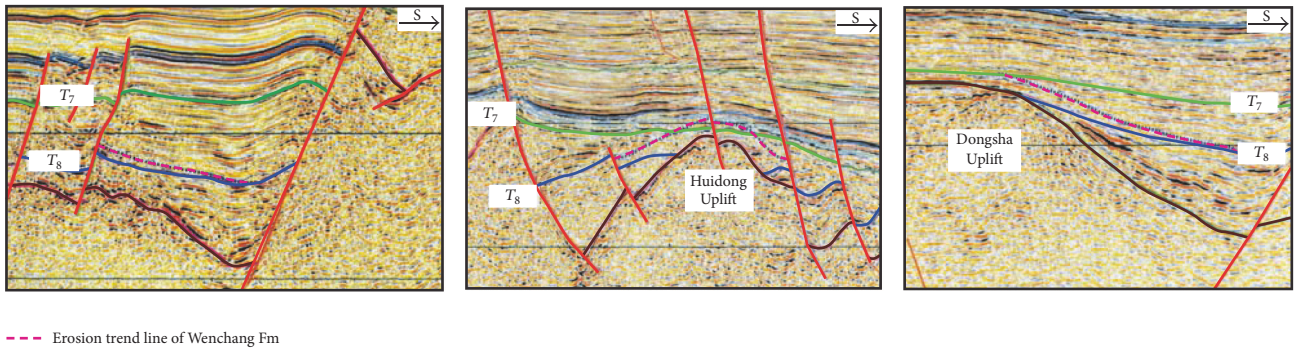

Figure 14: Method to estimate the erosion thickness in the Huizhou Sag [59] (the sequence boundaries are shown in Figure 2).

activation energy of 46~66 kcal/mole, showing a skewed distribution of the hydrocarbon generation potential. These results of our previous papers were adopted in this paper.

3.2.4. Geothermal Field and Boundary Conditions. Because present water depth is less than 200 m in the HZS, the variation of paleobathymetry has slight influence on the thermal evolution. The paleobathymetry is estimated according to the sedimentary facies characteristics (Table 6) in this paper and published literature [3].

The bottom hole temperature (BHT), surface temperature, and present heat flow were collected from boreholes and corrected according to Yuan et al. [62]. According to the recent researches [62–67], the current geothermal gradient of

Table 6: The estimated paleobathymetry according to the sedimentary facies characteristics.

Facies	Fluvial	Shore-shallow lacustrine	Deep lacustrine	Coastal	Shelf	Abyssal
Depth (m)	0	5~15	15~35	35~50	50~80	>80

the HZS ranges from 30.0°C/km to 36.0°C/km and increases from north to south.

Present-day basal heat flow is calculated from thermal conductivities of the rock units and geothermal gradients which is determined by measured BHT according the following equations:

$$\lambda_{\mathrm{MIX}} = \frac{\sum d_i}{\sum (d_i/\lambda_i)}, \tag{17}$$

where λ_{MIX} is the average conductivity of the sediment column (W/m·°C), d_i is the thickness of each lithology (m), and λ_i is the conductivity of each lithology (W/m·°C).

$$Q = \lambda_{\mathrm{MIX}} \times \frac{(T_B - T_0)}{\Delta Z}, \tag{18}$$

where Q is the basal heat flow at the bottom of the sedimentary pile (mW/m^2), T_0 is the temperature at the surface of the sediment column (°C), T_B is the temperature at the base of the sediment column (°C), and ΔZ is the sedimentary thickness from the surface to the base of the stratigraphic column (m).

The present-day basal heat flow of the HZS ranges from 51.2 mW/m^2 to 75.33 mW/m^2, with average of 62.98 mW/m^2 (Table 7). The paleoheat flow was applied in this study based on previous work [68–70]. Thermal evolution is calibrated by measured Ro and temperature values. The HZS shares similar thermal history due to the same rifting events. When the calculated basal heat flow value (54.5 mW/m^2) from well 131 was used as an input parameter in steady-state heat flow model to calculate the thermal history, the simulated maturity (Ro%) values and temperatures are much higher than the measured Ro values and measured BHT (Figure 15(a)). When the lower basal heat flow value (49.0 mW/m^2) was inputted into the same geologic model again, the new "simulated" Ro values fit the "measured" Ro values reasonably well, while the "simulated" temperature was much lower than measured BTH below 3500 meters (Figure 15(b)). After testing the steady-state heat flow method with constant heat flow of 54.5 and 49 mW/m^2 and a variable paleoheat flow (Figure 15(c)), the best fit between measured and calculated Ro and temperature was achieved by setting a variable paleoheat flow increasing from background value of 55 mW/m^2 [71, 72] to 73.84 mW/m^2 during the continental rift stage and then decreasing to the present heat value during the postrift stage (Figure 16). Thus, the steady heat flow method with was a variable paleoheat flow used to calculate geothermal history.

3.2.5. Pressure Field. Based on measured formation pressure, present pressure is characterized by normal pressure within most of the HZS (Figure 17(a)). The pressure of most drilled wells belongs to the range of normal pressure zone, with pressure coefficients ranging from 0.96 to 1.06 (Figure 17(b)).

Table 7: Newly measured geothermal data of the Huizhou Sag (HZS).

Well	Geothermal gradient (°C/km)	Average heat conductivity (W/(m·K))	Heat flow (mW/m^2)
81	30.3	2.07	62.65
131	30.0	1.82	54.50
181	35.5	1.97	70.00
211	33.9	2.07	68.60
2112	36.5	1.81	66.07
2311	32.6	1.86	60.64
257	35.5	1.68	59.60
2582	31.0	1.74	54.00
2583	32.4	1.58	51.20
261	36.3	1.90	68.90
268	33.2	1.70	56.44
274	34.8	1.82	63.34
321	30.4	2.06	62.70
331	33.1	1.92	63.70
241	29.8	2.02	59.30
243	30.0	1.98	60.20
2432	29.7	1.90	56.90
302	34.7	1.80	62.46
131	41.2	1.76	72.51
1312	42.8	1.76	75.33
132	38.7	1.87	72.56
142	38.3	1.79	68.56

There is no obvious overpressure in the well 132, well 81, and well 241 (Figures 17(c), 17(d), and 17(f)), and formation pressure is equal to the hydrostatic of normal pressure zone. As the buried depth increased, formation pressure curve of well 131 gradually deviates from the hydrostatic pressure, and slight overpressure develops in the lower Zhujiang Fm, Zhuhai Fm, and Enping Fm (Figure 17(e)).

4. Results and Discussion

Two 2D models were constructed based on seismic data and drilling well data. The variation of paleoheat flow calibrated from 1D modeling was adopted in the 2D model to simulate the process of migration and accumulation of hydrocarbon fluids in the HZS [48].

4.1. Maturity History, Petroleum Generation, and Expulsion

4.1.1. Burial and Thermal History. Since the selected wells are situated in the structural high, the mature level of the

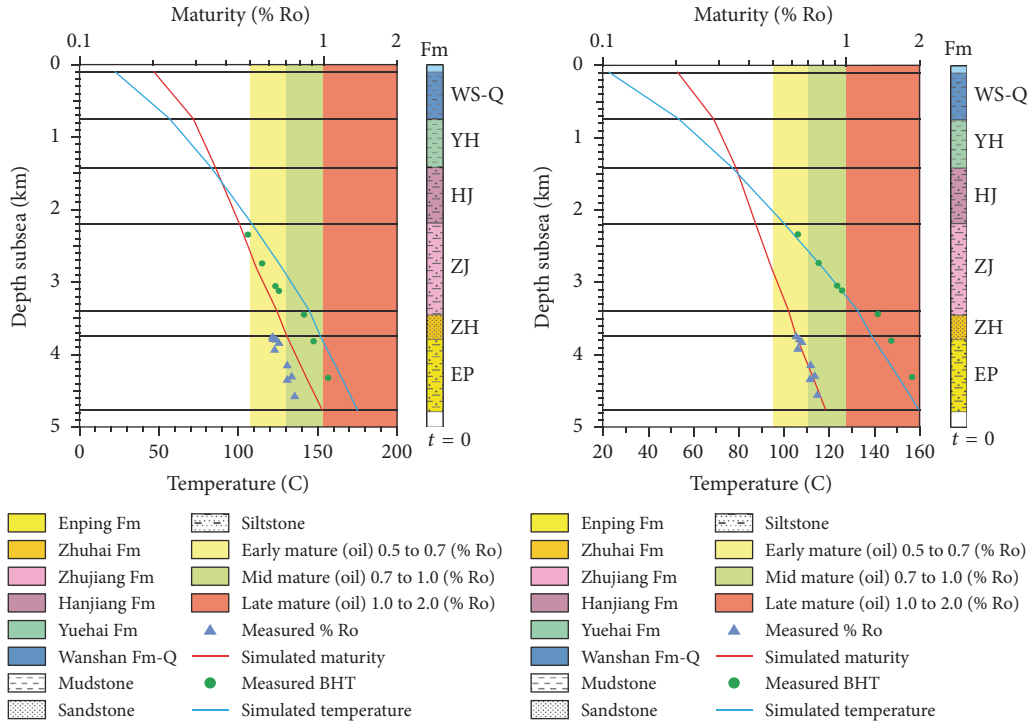

(a) Steady-state heat flow model with 54.5 mW/m^2

(b) Steady-state heat flow model with 49.0 mW/m^2

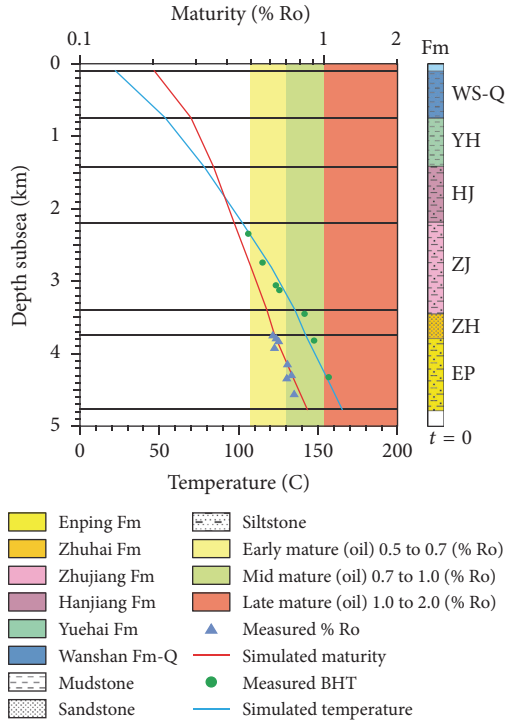

(c) Steady-state heat flow model with variable basal heat flow

Figure 15: Fitting results between measured and simulated Ro and temperature of well 131 under different heat flow models. The locations of well 131 are shown in Figure 1 (formation names: EP = the Enping Fm; ZH = the Zhuhai Fm; ZJ = the Zhujiang Fm; HJ = the Hanjiang Fm; Yh = the Yuehai Fm; WS = the Wanshan Fm; Q = Quaternary).

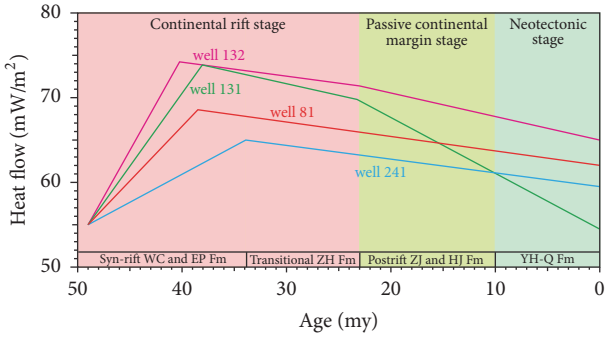

FIGURE 16: Variable paleoheat flow model applied in Transient Heat Flow Method of the Huizhou Sag (the locations of wells are shown in Figure 1).

Eocene source rocks is generally in the early-main nature stage. The well 81 with total depth of 4583.0 m, located in the northern part of the HZS, has drilled into the Eocene Enping Fm. The drilling data were used to establish geologic model for studying the thermal history (Figure 18(a)). The Eocene Enping source rocks are currently in a main mature stage. After the rapid subsidence during the Eocene continental rift stage, the Eocene Enping source rocks entered the early mature stage at 18.5 Ma. With the increase of buried depth, the Eocene Enping Fm further evolved into the main mature stage, with the EASY % Ro ranging from 0.7% to 1.0% during the period from 9.5 Ma to the present. The bottom of the Miocene Zhujiang and Oligocene Zhuhai Fm is currently in an early mature stage.

The well 131 with a total depth of 4804.0 m, located in the central part of the HZS, has drilled into the Eocene Enping Fm. The lithological data obtained from drilling well were used to establish geologic model, from which a better fit between measured and calculated Ro was obtained (Figure 18(b)). The burial and thermal history is quite similar to that of the well 81. The Eocene Enping source rocks are currently in an early-main mature stage, with Ro values ranging from 0.6% to 0.9%. The Eocene Enping Fm evolved into the main mature stage after 9.5 Ma. The upper part of the Eocene Enping source rocks is currently in an early mature stage, and the lower part is in a main mature stage. The lower part of the Miocene Zhujiang and Oligocene Zhuhai Fm is also currently in an early mature stage.

The well 241 with a total depth of 3853.1 m, located in the southern margin of the HZS, has drilled into the Pre-Cenozoic granite. Because this well is located in the uplift area, approximately 1 km of the Eocene Wenchang Fm and whole Enping Fm were eroded due to the Zhu-Qiong II and Nanhai Movement (Figure 18(c)). There is only 165 m thickness of the Eocene Wenchang Fm preserved. The Eocene Wenchang source rocks are currently in an early mature stage, with Ro values ranging from 0.45% to 0.75%, which entered the early mature stage at 12.0 Ma. The lower part of the Miocene Zhujiang and Oligocene Zhuhai Fm is also currently in an early mature stage.

The water depth of well 132 is deeper than that of above three wells, which is located in the Huilu low-uplift. The oldest layer is the Eocene Wenchang Fm with a total drilling depth of 3280.0 m. The thickness of the Eocene Enping and Wenchang Fm is estimated from drilling data. Because of regional tectonic uplift movement, about 400 m of the Eocene Wenchang Fm and 100 m of the Eocene Enping Fm are eroded. It is shown from the simulated results (Figure 18(d)) that the Eocene Wenchang and Enping Fm are currently in a marginally mature stage, with Ro values ranging from 0.5% to 0.6%, and the overlying strata are all in the immature stage (Ro < 0.5%). The Eocene Wenchang and Enping source rocks evolved into the early mature stage at 9.0 Ma.

The Eocene source rocks in the deeper sag are generally in the late-mature stage, with Ro value more than 2.0% (Figures 19(a) and 19(b)). The maturity level in the Huilu low-uplift (Figure 19(c)) is lower than that in the Huixi half-graben (Figure 19(c)). Most of the generated hydrocarbon is from the Eocene Wenchang and Enping source rocks in the deep part of the HZS.

4.1.2. Timing of Hydrocarbon Generation and Expulsion. The hydrocarbon generation process of the Eocene source rocks was simulated using four wells as examples. "Oil" and "gas" in this paper refer to the composition of generated fluids/hydrocarbons. The Eocene Enping source rock of well 81 is mainly in hydrocarbon generation stage, with oil and gas generation amount of 78 mg/g·TOC and 118 mg/g·TOC, respectively (Figure 20(a)). The first stage (approximately 36.0–18.5 Ma) is a minor phase of hydrocarbon generation without any hydrocarbon expulsion. The second stage (from 18.5 Ma to present) is the phase of major hydrocarbon generation and expulsion. The hydrocarbon expulsion began at 18.5 Ma, expelled little in the second stage because of low maturity level of the source rocks. Because of lower maturity level of the Eocene Enping source rocks, the hydrocarbon generation amount is relatively low in well 131, with present oil and gas generation amount of 16.8 mg/g·TOC and 29 mg/g·TOC, respectively (Figure 20(b)). The hydrocarbon expulsion also began at 18.5 Ma but was expelled little. The present hydrocarbon generation amount of well 241 is less than 30 mg/g·TOC, and hydrocarbon expulsion began at 14.0 Ma but was rarely expelled (Figure 20(c)). In general, the hydrocarbon generation and expulsion of the Eocene source rocks on structural high are not high, which is because of the location of structural high and low maturity level.

The situation in the deep part of the HZS is different. The period of large hydrocarbon generation of the Enping source rocks in the Huibei half-graben is generally in the thermal subsidence stage and mainly occurred within the last 20 Ma (Figures 20(e) and 20(f)). Hydrocarbon expulsion of the Enping Fm began at 33.9 Ma but was rarely expelled. The period of large hydrocarbon generation of the Wenchang source rocks in the Huixi half-graben is earlier than that in the Huibei half-graben, which started mainly at 33.9 Ma (Figures 20(g) and 20(h)). The modeling results indicate that hydrocarbon generation potential of the Wenchang Fm in the Huixi half-graben is much higher than that in the Huibei half-graben, with oil generation potential of 70 mg/g·TOC and gas generation potential of around 150 mg/g·TOC. Hydrocarbon expulsion of the Wenchang Fm began at 33.9 Ma and was

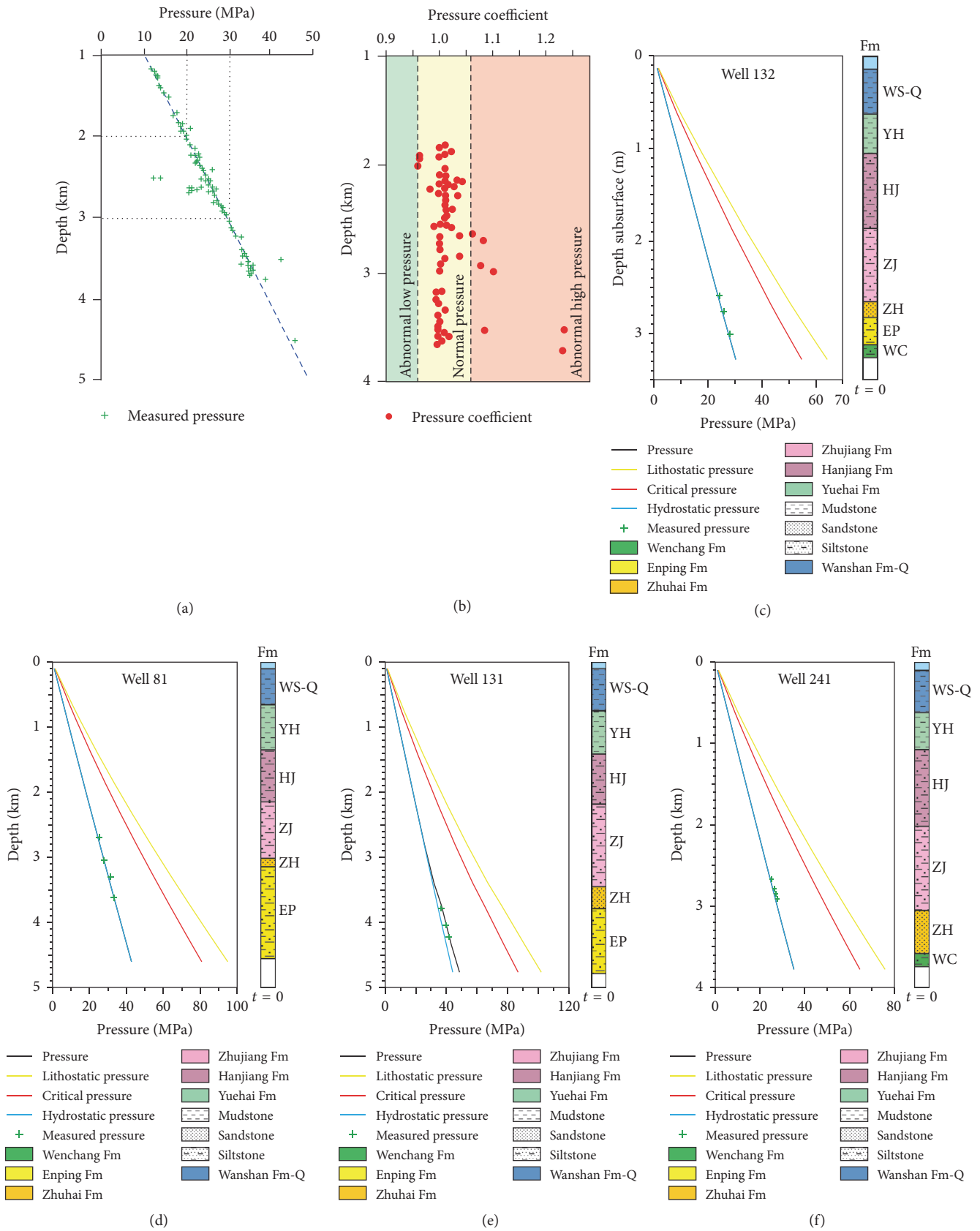

FIGURE 17: Pressure field (a), pressure coefficient (b), and pressure fitting of wells (c–f) in the Huizhou Sag. The locations of four wells are shown in Figure 1 (formation names: EP = the Enping Fm; ZH = the Zhuhai Fm; ZJ = the Zhujiang Fm; HJ = the Hanjiang Fm; Yh = the Yuehai Fm; WS = the Wanshan Fm; Q = Quaternary).

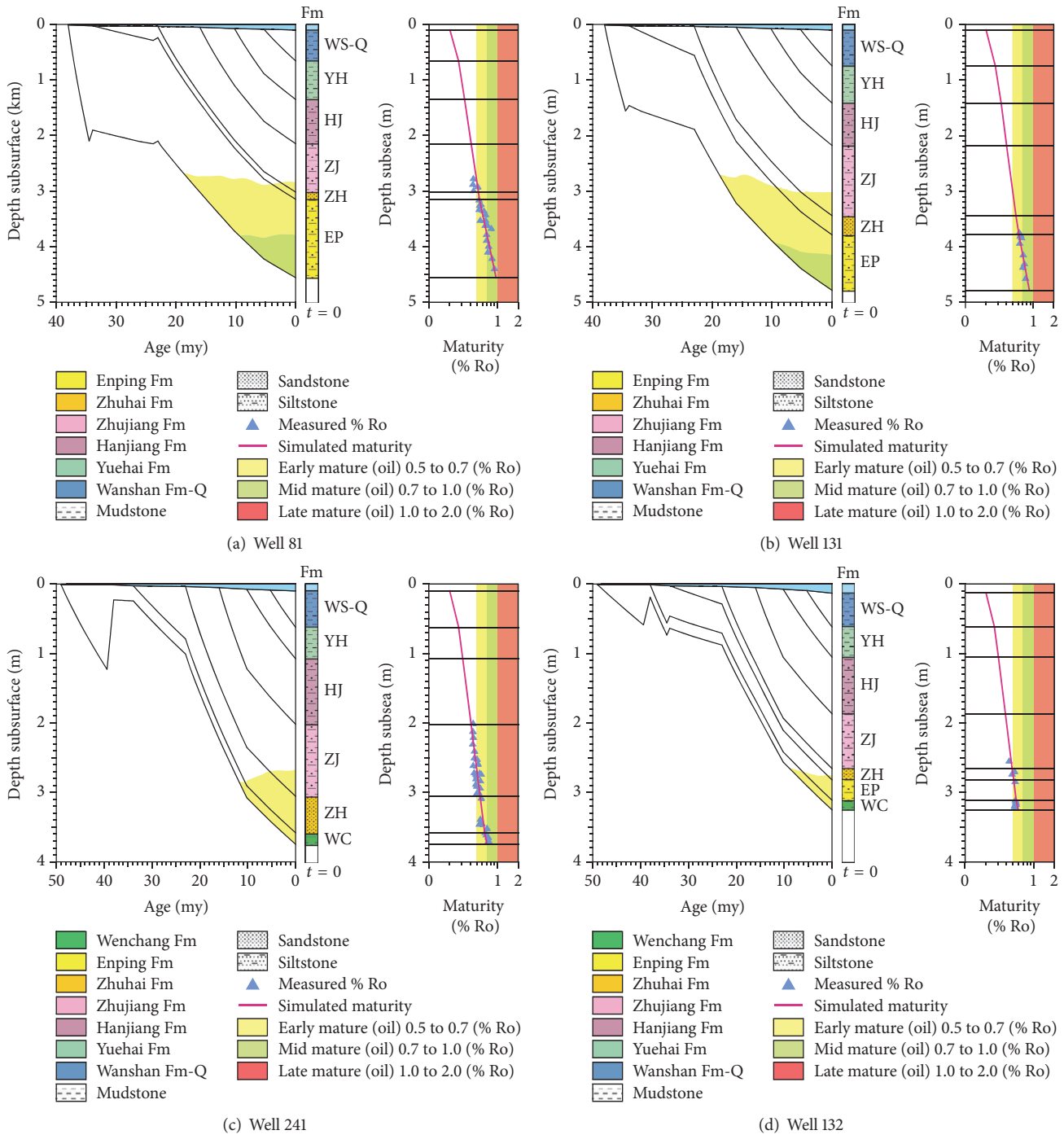

Figure 18: Modeling burial-thermal history calibrated by the measured Ro in the Huizhou Sag (the locations of four wells are shown in Figure 1). Formation names: WC = the Eocene Wenchang Formation; EP = the Eocene Enping Formation; ZH = the Oligocene Zhuhai Formation; ZJ = the Miocene Zhujiang Formation; HJ = the Miocene Hanjiang Formation; YH = the Miocene Yuehai Formation; WS-Q = the Pliocene Wanshan Formation to Quaternary.

expelled much more (Figures 20(g) and 20(h)). The oil expelled volume reaches 11 mg/g rock in the center of the Huixi half-graben (Figure 20(h)).

4.2. Petroleum Migration and Accumulation Modeling. In this study, short and long distance migration of the Eocene petroleum have been predicted for the hydrocarbon accumulation in the HZS. Most hydrocarbons generated from the deep Eocene source rocks of the HZS started to generate from 33.9 Ma and shallower source rocks are still generating hydrocarbons. Previous research indicated that most petroleum of oil field originated from the deep lacustrine

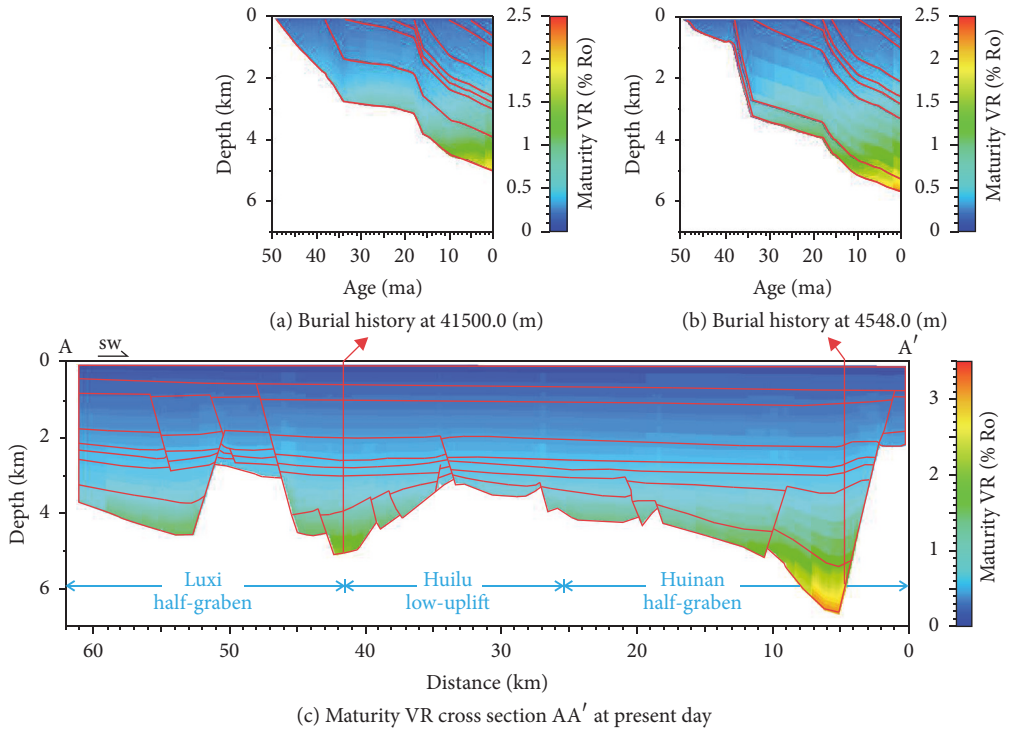

FIGURE 19: Modeled thermal maturity expressed as vitrinite reflectance (% Ro) in the Huilu low-uplift area (the locations of the profile AA′ are shown in Figure 1).

Wenchang dark mudstone and shoreline-shallow lacustrine Enping dark mudstone and accumulated via lateral migration from the deeply buried source rocks in the HZS [2, 3, 43, 44, 47]. The modeling results indicate that oil expulsion in the HZS is mainly from the Eocene Wenchang source rocks and occurred during postrift stage. The shaly facies of the upper Zhujiang Fm and overlying strata acted as an effective seal rock for the lower Zhujiang and Zhuhai sandy reservoirs, limiting the vertical migration of hydrocarbons from these reservoirs towards higher stratigraphic intervals.

In the eastern HZS, petroleum mainly accumulated not only in structural highs of the shallow Zhujiang and Zhuhai Fm, but also in the deep Wenchang Fm (Figure 21(a)). Petroleum accumulated in the Zhujiang and Zhuhai Fm generally started at 10 Ma, with different oil accumulated volume in different area. In the Huilu low-uplift, oil accumulated volume reached 0.08 m^3/m^3 at present day (Figures 21(c) and 21(e)). Petroleum accumulated in the southwest of the Luxi half-graben is relatively high (Figures 21(d) and 21(f)), and oil accumulated volume exceeded 0.10 m^3/m^3 at 5.3 Ma (Figure 21(d)). Petroleum generated from the Eocene Wenchang source rocks began to accumulate in the adjacent Wenchang reservoirs from 16 Ma. The maximum accumulated oil volume in the Luxi half-graben and the Huinan half-graben is both around 0.055 m^3/m^3 at 5.3 Ma (Figures 21(g) and 21(h)). LF13-2 oil field (Figure 21(i)) was successfully discovered with proven geological reserves of 6.05×10^6 m^3 [38]. Hydrocarbon sourced from the Wenchang Fm migrated from north area via the Zhuhai and Zhujiang carrier and faults to the LF13-2 structural high (Figure 21(j)).

In the Huibei half-graben, hydrocarbons mainly accumulate on the top of the Wenchang and Enping Fm, which have three-stage accumulations (Figure 22(a)). The first stage occurred from 33.9 Ma to 21 Ma with no more than 0.01 m^3/m^3 oil accumulated. The second stage occurred from 14 Ma to 11 Ma, with more than 0.038 m^3/m^3 oil accumulated. The third stage started at 5.0 Ma, with accumulated oil of 0.051 m^3/m^3 (Figure 22(g)). Petroleum currently accumulated in a series of strata, including Wenchang, Enping, Zhuhai, and Zhujiang Fm in the Huixi half-graben (Figure 22(a)). The modeling results indicate that the main period of hydrocarbon accumulation in the Zhujiang Fm is from 5.0 Ma to present day, with oil accumulated volume of 0.045 m^3/m^3 (Figure 22(c)). The Zhuhai Fm has two-stage petroleum accumulations. First stage is from 16.0 Ma to 11.0 Ma with more than 0.02 m^3/m^3 oil accumulated, and second stage started from 10.0 Ma with more than 0.02 m^3/m^3 oil accumulated (Figures 22(d) and 22(e)). Furthermore, hydrocarbons generated from the Eocene source rocks also migrated to the adjacent reservoirs and accumulated in the Wenchang and Enping Fm. Oil accumulated in the Enping Fm started from 15 Ma and temporarily ceased at 11 Ma, and then accumulation started again from 10 Ma to present day (Figure 22(f)). Petroleum accumulated in the Wenchang Fm began at 14 Ma, and accumulated oil volume reached peak of 0.048 0.02 m^3/m^3 at 10 Ma (Figure 22(h)).

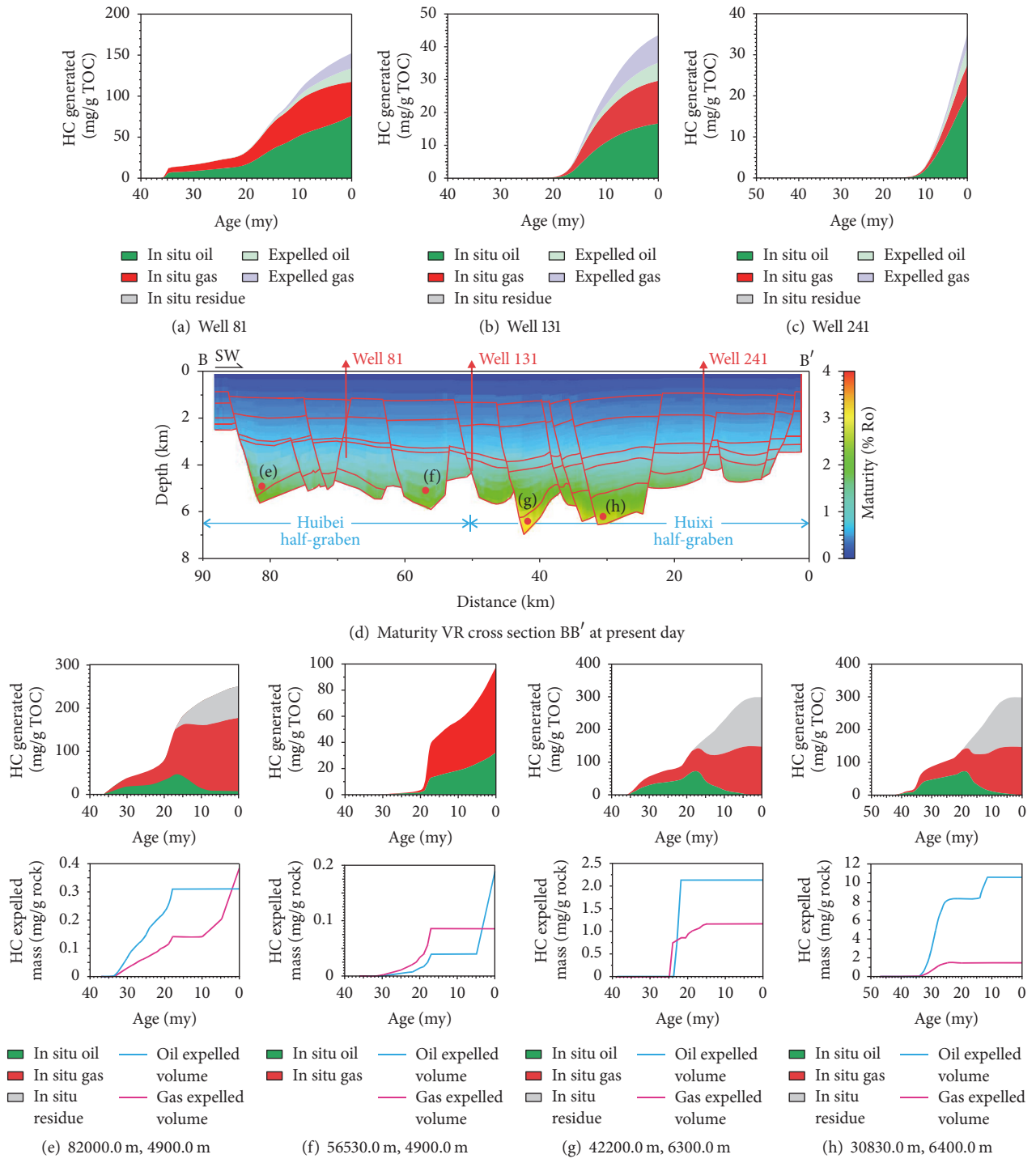

FIGURE 20: Hydrocarbon generation and expulsion of the Eocene source rocks in the Huizhou Sag (the locations of three wells and profile BB′ are shown in Figure 1).

From migration modeling results, the most likely fluid migration pathways are from the center of the depression to the flanks (Figure 22(a)) and structural high (Figure 21(a)), and the main driving forces for secondary petroleum migration are buoyancy and excess pressure caused by hydrocarbon generation of the deep source rocks (Figure 22(b)) and regional cap rocks (Figure 21(b)).

Faults are also important conduits for the Eocene source rocks to expel hydrocarbons towards traps in the structural high. Most major faults acted as migration pathways during the Eocene rift stage and then became sealed during the postrift stage. After that, previous reactivated faults and newly formed faults, resulting from the Dongsha Movement (9.8–4.4 Ma), served as migration pathways for petroleum.

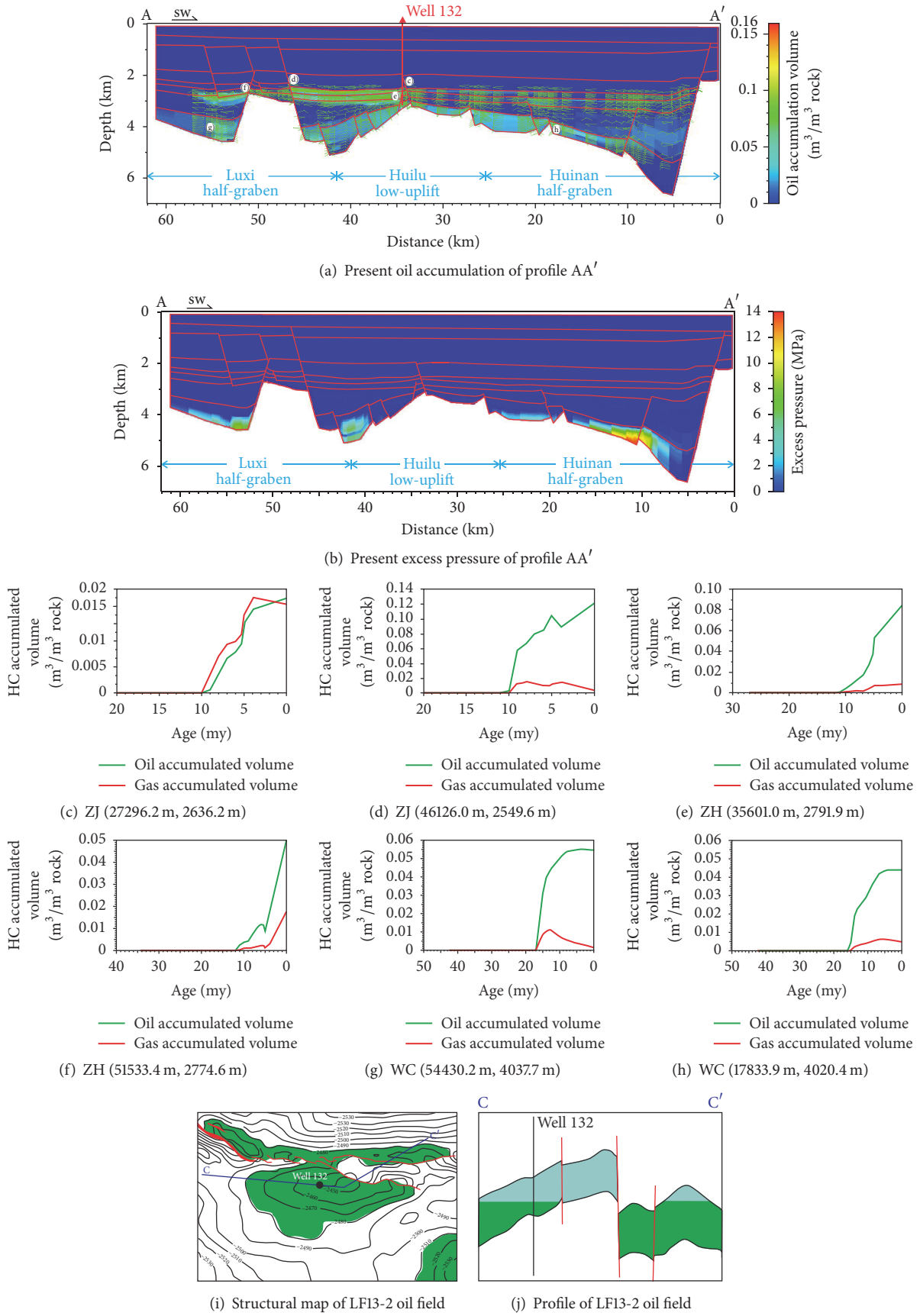

(a) Present oil accumulation of profile AA′

(b) Present excess pressure of profile AA′

(c) ZJ (27296.2 m, 2636.2 m)

(d) ZJ (46126.0 m, 2549.6 m)

(e) ZH (35601.0 m, 2791.9 m)

(f) ZH (51533.4 m, 2774.6 m)

(g) WC (54430.2 m, 4037.7 m)

(h) WC (17833.9 m, 4020.4 m)

(i) Structural map of LF13-2 oil field

(j) Profile of LF13-2 oil field

Figure 21: Hydrocarbon fluid migration and accumulation of the Eocene source rocks in the Huilu low-uplift area (calculated hydrocarbon volume is expressed in reservoir condition. The locations of well 132 and profile AA′ are shown in Figure 1).

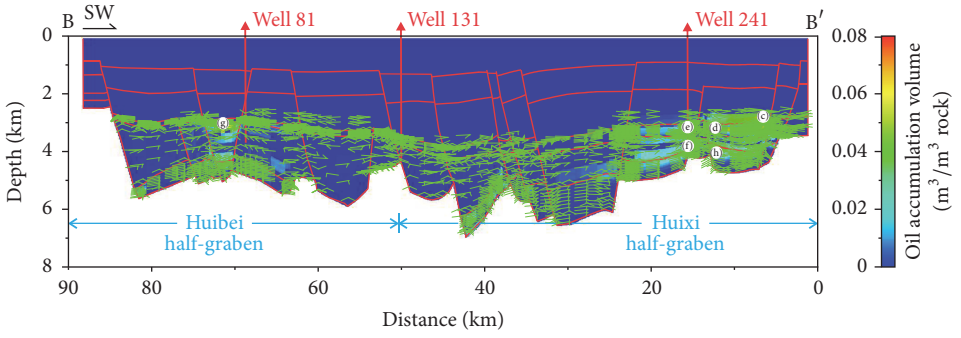

(a) Present oil accumulation of profile BB′

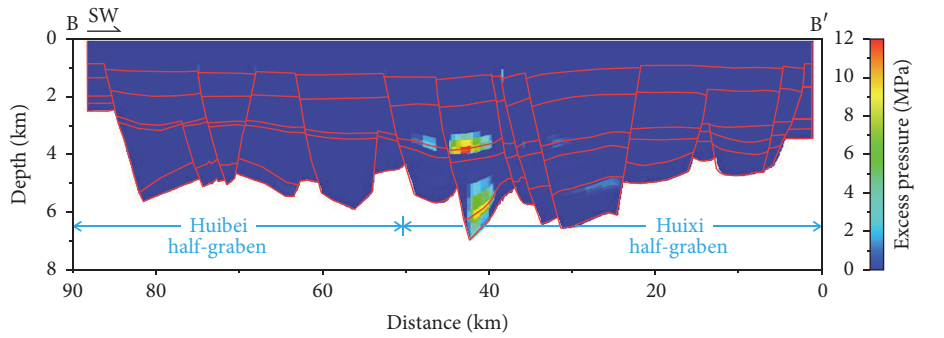

(b) Present excess pressure of profile BB′

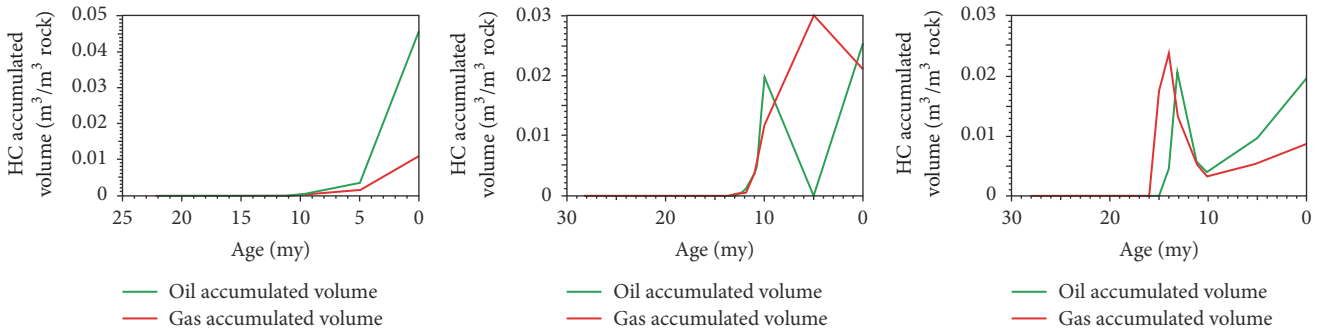

(c) ZJ (6535.6 m, 2867.2 m) (d) ZH (12898.2 m, 3174.5 m) (e) ZH (15732.5 m, 3264.8 m)

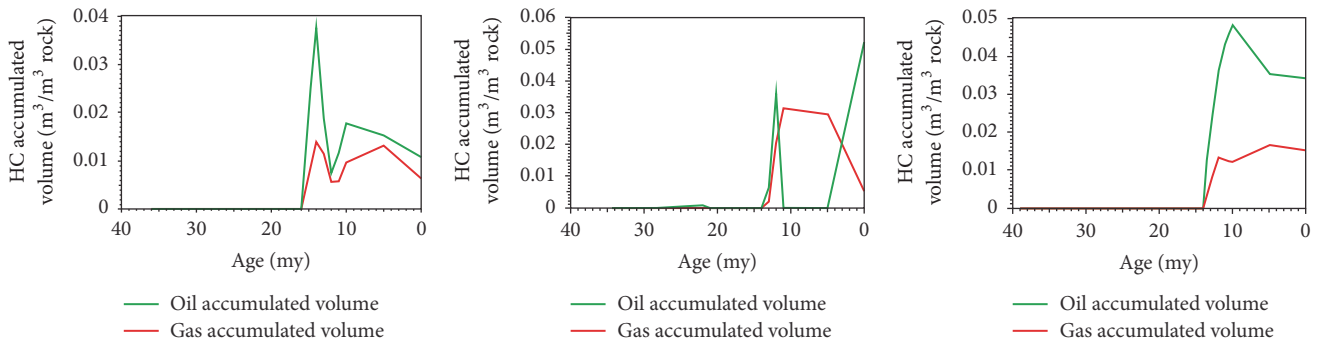

(f) EP (15616.8 m, 3752.8 m) (g) EP (71666.0 m, 3120.2 m) (h) WC (12840.4 m, 3807.0 m)

Figure 22: Hydrocarbon fluid migration and accumulation of the Eocene source rocks in the Huixi and Huibei half-graben (calculated hydrocarbon volume is expressed in reservoir condition. The locations of three wells and profile BB′ are shown in Figure 1).

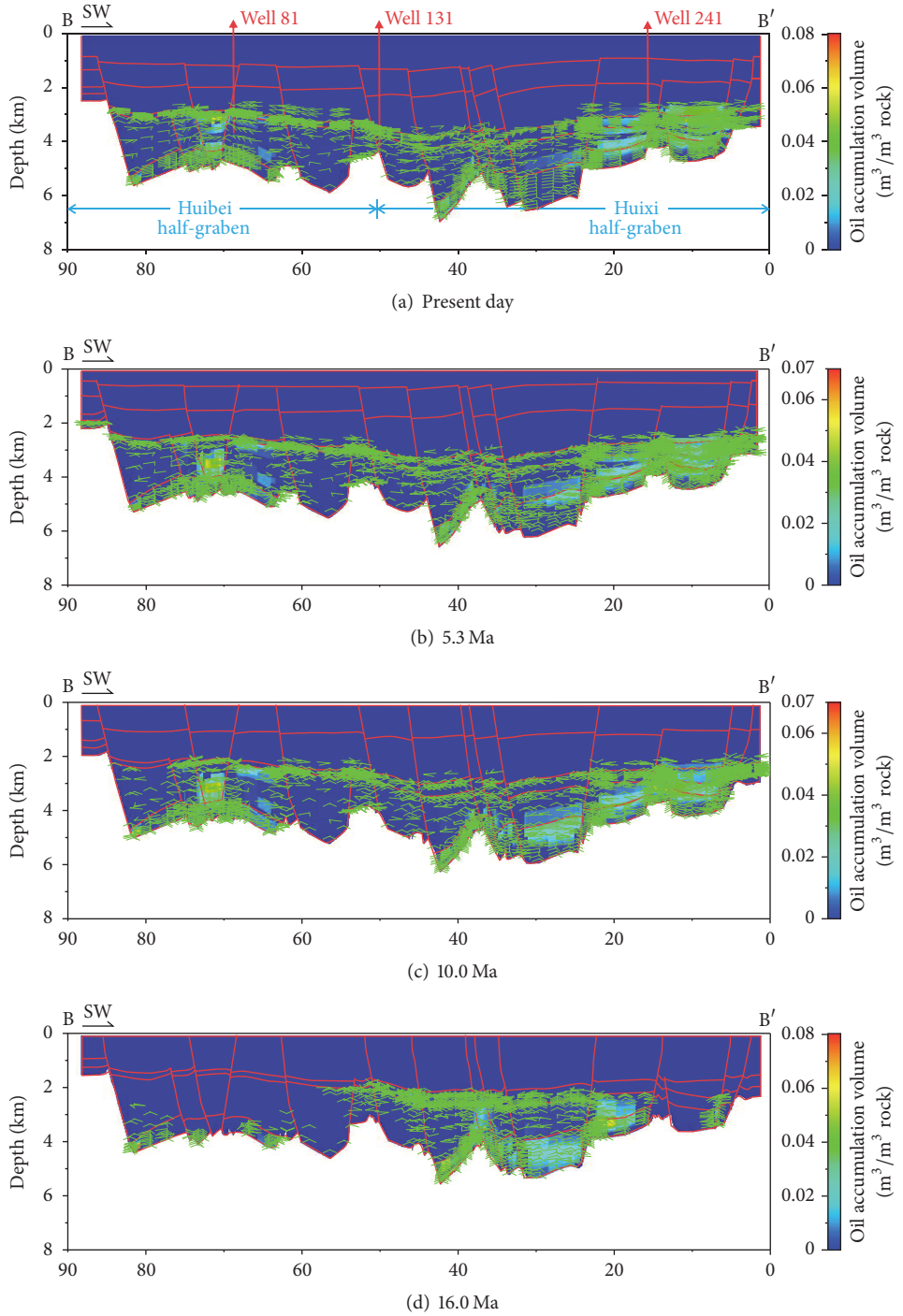

Figure 23: Dominant hydrocarbon fluid pathway and accumulation model of the Eocene source rocks during postrift and block faulting stage in the Huizhou Sag (the locations of three wells and profile BB′ are shown in Figure 1).

The hydrocarbon fluids accumulated in the deep Eocene reservoirs interval and then vertically migrated up to the overlying postrift strata via faults and then laterally migrated to the adjacent reservoirs via the homogeneous carrier beds (Figure 23(c)). The continuous homogeneous Zhuhai and Zhujiang sandstone, combined with structural highs, was considered to act as major pathways for long distance hydrocarbon migration in the HZS (Figure 23(b)).

4.3. Sensitivity Analysis. The crucial parameters were selected for parameter sensitivity analysis of the basin modeling. The sensitivity simulation suggests that paleogeothermal

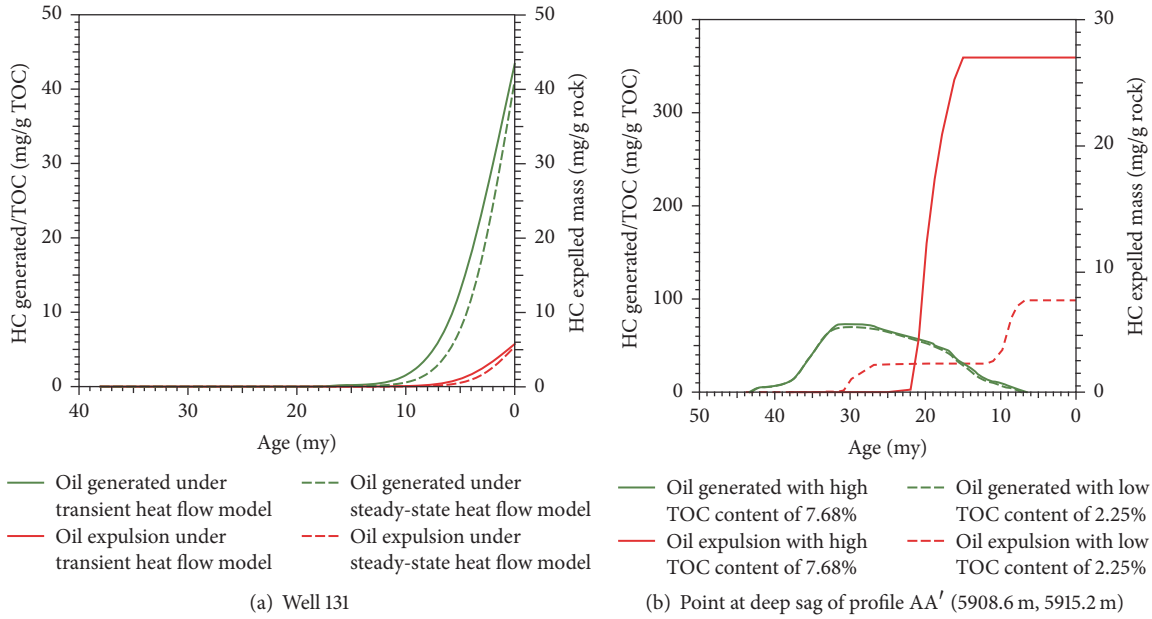

Figure 24: Sensitivity analysis of heat flow model (a) and TOC content in the Huizhou Sag (the location of well 131 is shown in Figure 1).

history affects hydrocarbon generation-expulsion histories, total organic carbon content of source rocks affects hydrocarbon expulsion, the permeability of fault zones strongly affects excess pressure in the deep sag, and the reservoir continuity significantly affects hydrocarbon accumulation.

4.3.1. Effect of Paleogeothermal History and TOC Content of Source Rocks on Hydrocarbon Generation-Expulsion Histories. Well 131 was selected to test the sensitivity of hydrocarbon generation-expulsion histories under different heat flow model. Although the amount of the generating and expelling hydrocarbon was the same, the process was slight different (Figure 24(a)). Moreover, the TOC content of source rocks also affects hydrocarbon generation-expulsion process, even though the generated hydrocarbons so far are the same (Figure 24(b)).

4.3.2. Excess Pressure. According to the measured pressure data (Figure 17), overpressure generally does not develop in the HZS. The seal capability of fault zones is considered to be the main controlling factor based on our interacted analysis. A boundary from profile AA′ was selected to analyze the overpressure condition under the different permeabilities of fault zones. Leak fraction is used to present permeability of all faulted cell in BasinMod 2D. No matter how the leak fraction was set, there was not much difference between the excess pressure when the boundary fault was set as permeable fault (Figures 25(a) and 25(b)). However, when the leak fraction was set to 0, which means that the fault was impermeable, the excess pressure in the Huinan half-graben was much higher than that with permeable boundary fault (Figure 25(c)). Hence, permeability of fault zones strongly affects the pressure field in the deep sag.

4.3.3. Reservoir Continuity. A thin continuous sand body was built at the bottom of Zhuhai Fm to test the sensitivity of continuous reservoir. When the lithology was set as pure sandstone, much more oil has migrated through continuous reservoir into the shallower Zhuhai and Zhujiang Fm (Figure 26(a)). However, when the lithology was set as a stratum with laterally variable lithology, most hydrocarbons migrating will be trapped in the deep Wenchang and Enping Fm close to the source rocks for the heterogeneous reservoirs (Figure 26(b)).

5. Conclusion

Basin modeling was conducted for four representative wells and two profiles in the Huizhou Sag (HZS) to reconstruct the process of generation, expulsion, migration, and accumulation hydrocarbon in Cenozoic Period since midcontinental rifting started in Eocene.

(1) The Eocene Wenchang source rocks consist of shoreline-shallow lacustrine and deep lacustrine dark mudstone, and the kerogen is mainly of Type-II_1, with minor component of Type-I. The Eocene Enping source rocks consist of swamp mudstone, swamp carbonaceous mudstone, and fluvial-delta mudstone and are generally composed of Type-II_1 and Type-II_2 kerogen.

(2) The Eocene source rocks deposited in rift stage are currently in a middle-mature and late-mature stage, with % Ro value ranging from 0.7% to 3.0%. The Eocene source rocks developed in structural highs entered early mature stage at 23.0 Ma, while source rocks developed in deep central part of the sag have been in mature stage after 33.9 Ma. The Eocene source rocks started to generate hydrocarbons at 33.9 Ma. Hydrocarbon generation potential of the Wenchang source

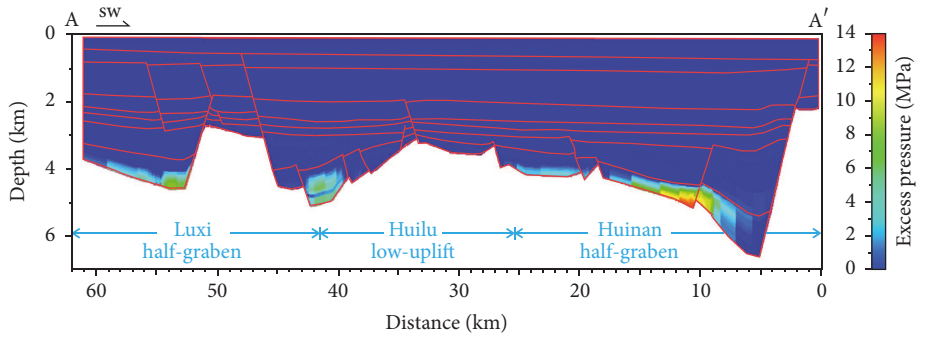

(a) Present excess pressure with permeable boundary fault (leak fraction = 1)

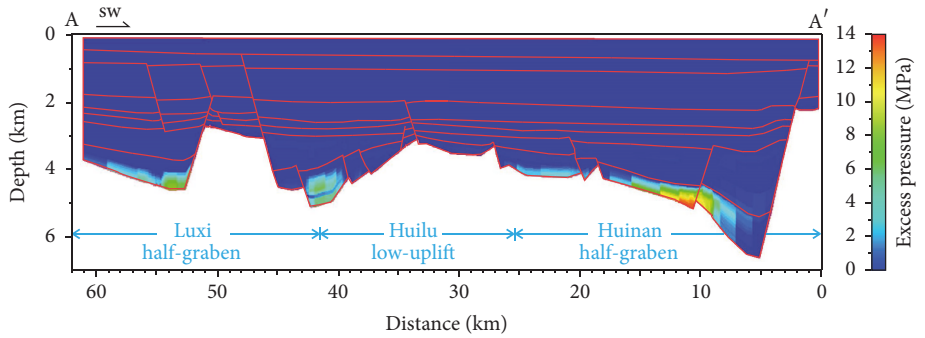

(b) Present excess pressure with permeable boundary fault (leak fraction = 0.5)

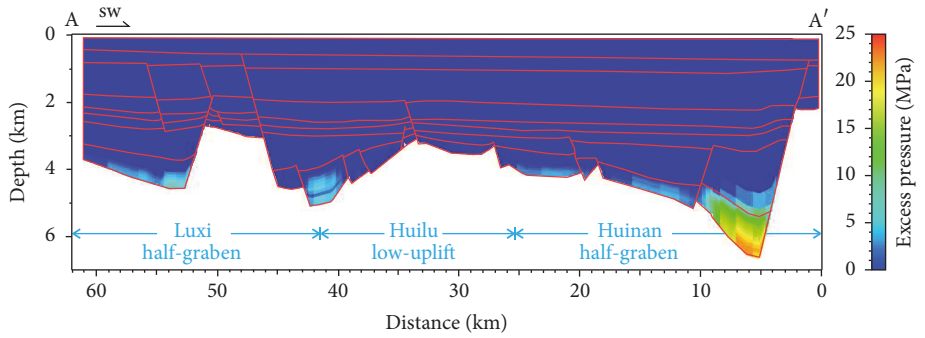

(c) Present excess pressure with impermeable boundary fault (leak fraction = 0)

Figure 25: Sensitivity analysis of permeability of fault zones in the Huizhou Sag (the location of profile AA′ is shown in Figure 1).

rock is much higher than that of the Enping source rock. Hydrocarbons were mainly expelled from the Wenchang Fm, and the contribution from the Enping Fm is relatively low.

(3) Both short and long distance hydrocarbon migrations of the Eocene source rocks occurred in the HZS. Short distance hydrocarbon migration occurred in the Eocene reservoirs and is characteristics of multiperiod accumulation, while long distance hydrocarbon migration generally occurred in the Oligocene Zhuhai and Miocene Zhujiang reservoirs, which started to accumulate through 20~50 km homogeneous carrier beds after 10.0 Ma.

(4) The hydrocarbons generated from the Eocene source rocks firstly migrated laterally to the adjacent Eocene reservoirs during the postrift stage, then vertically to the Oligo-Miocene carrier beds, and finally laterally through a long distance to the structural highs during the Neotectonic stage, which is controlled by both structural morphology and heterogeneity of carrier beds.

(5) Fault is the most important conduit for hydrocarbon migration during the Neotectonic stage. Reactivation of previously existing faults and new-formed faults, caused by the Dongsha Movement (9.8–4.4 Ma), served as vertical migration pathways, which significantly influenced the timing of hydrocarbon accumulation in the postrift traps.

(6) According to the sensitivity simulation of different factors, source rocks with high total organic carbon (TOC) content in the deeper sag could expel more hydrocarbons. Zones with impermeable faults are more likely to generate high excess pressure in the deeper sag. The continuous homogeneous reservoir contributes to hydrocarbon migration from the deep source rocks to shallow reservoir in the HZS.

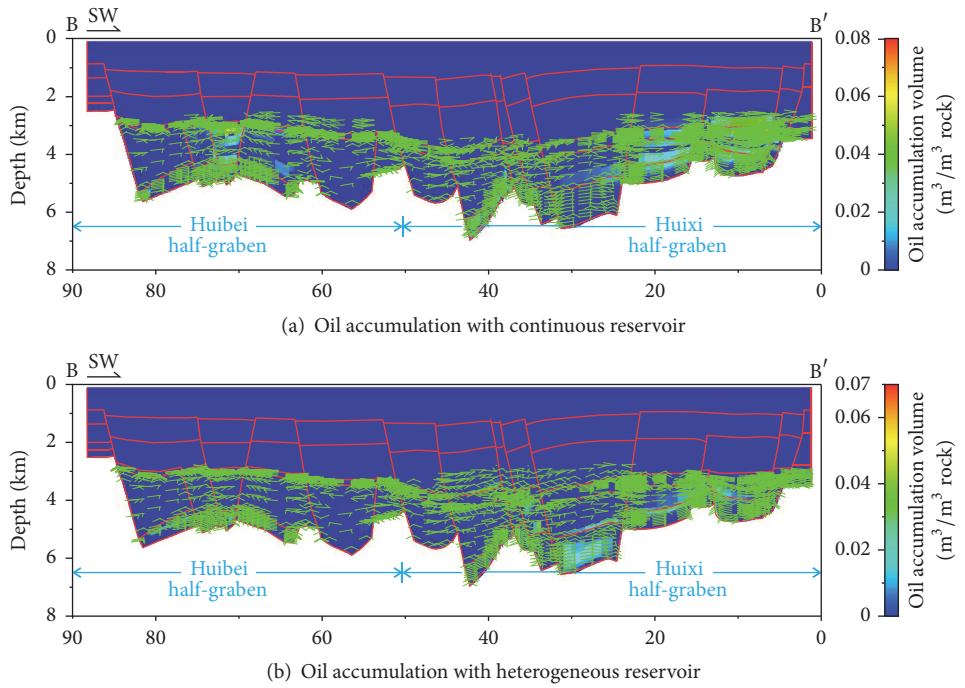

Figure 26: Sensitivity analysis of continuity of reservoir in the Huizhou Sag (the location of profile BB′ is shown in Figure 1).

Conflicts of Interest

The authors declare that they have no conflicts of interest.

Acknowledgments

This work was supported by integrated research project, The Paleogene Sequence Stratigraphy and Conditions of Hydrocarbon Accumulation in Zhu 1 Depression, Pearl River Mouth Basin, sponsored financially by China National Offshore Oil Corporation (2009GYXQ02-06) and National Natural Science Foundation of China (Grant no. 41106108).

References

[1] J. M. Yang, K. Q. Wu, and X. C. Yang, "Research on multiphase hydrocarbon migration of mixed source rocks in a long distance through main pathway in the Huizhou Sag," in *Hydrocarbon Accumulation Dynamics Research of The Northern Continental Margin Basin of The South China Sea*, Z. S. Gong and S. T. Li, Eds., pp. 223–225, China Sciences Press, Beijing, China, 2004.

[2] J. Peng, X. Pang, H. Peng et al., "Geochemistry, origin, and accumulation of petroleum in the Eocene Wenchang Formation reservoirs in Pearl River Mouth Basin, South China Sea: A case study of HZ25-7 oil field," *Marine and Petroleum Geology*, vol. 80, pp. 154–170, 2017.

[3] J. Peng, X. Pang, H. Shi et al., "Hydrocarbon generation and expulsion characteristics of Eocene source rocks in the Huilu area, northern Pearl River Mouth basin, South China Sea: Implications for tight oil potential," *Marine and Petroleum Geology*, vol. 72, pp. 463–487, 2016.

[4] T. T. Schowalter, "Mechanics of secondary hydrocarbon migration and entrapment," *AAPG Bulletin*, vol. 63, no. 5, pp. 723–760, 1979.

[5] W. A. England, A. S. Mackenzie, D. M. Mann, and T. M. Quigley, "The movement and entrapment of petroleum fluids in the subsurface.," *Journal of the Geological Society*, vol. 144, no. 2, pp. 327–347, 1987.

[6] W. A. England, "Secondary migration and accumulation of hydrocarbons," in *The Petroleum System-From Source to Trap*, L. B. Magoon and W. G. Dow, Eds., vol. 60, pp. 211–217, AAPG Memoir, 1994.

[7] A. D. Hindle, "Petroleum migration pathways and charge concentration: a three-dimensional model," *The American Association of Petroleum Geologists Bulletin*, vol. 81, no. 9, pp. 1451–1481, 1997.

[8] A. D. Hindle, "Downthrown traps of the NW Witch Ground Graben, UK North Sea," *Journal of Petroleum Geology*, vol. 12, no. 4, pp. 405–418, 1989.

[9] A. D. Hindle, "Petroleum migration pathways and charge concentration: a three-dimensional model," *AAPG Bulletin*, vol. 81, pp. 1020–1023, 1999.

[10] W. C. Gussow, "Differential entrapment of oil and gas: a fundamental principle," *AAPG Bulletin*, vol. 38, pp. 816–853, 1954.

[11] W. C. Gussow, "Migration of Reservoir Fluids," *Journal of Petroleum Technology*, vol. 20, no. 4, pp. 353–365, 2013.

[12] J. A. Momper, "Oil migration limitations suggested by geological and geochemical considerations: physical and chemical constraints on petroleum migration," *AAPG Bulletin*, vol. A034, pp. T.1–T.60, 1978.

[13] J. A. Momper and J. A. Williams, "Geochemical exploration in the Powder River basin," in *Petroleum Geochemistry and Basin Evaluation*, G. D. Demaison and R. J. Murris, Eds., vol. 35, pp. 181–191, AAPG Memoir, 1984.

[14] B. P. Tissot and D. H. Welte, *Petroleum Formation and Occurrence*, Springer, Berlin, Germany, 2nd edition, 1984.

[15] H. Dembicki Jr. and M. J. Anderson, "Secondary migration of oil: experiments supporting efficient movement of separate,

buoyant oil phase along limited conduits," *The American Association of Petroleum Geologists Bulletin*, vol. 73, no. 8, pp. 1018–1021, 1989.

[16] J.-C. Pratsch, "Gasfields, NW German Basin: secondary gas migration as a major geologic parameter.," *Journal of Petroleum Geology*, vol. 5, no. 3, pp. 229–244, 1983.

[17] J. C. Pratsch, "The distribution of major oil and gas reserves in regional basin structures-an example from the Powder River basin, Wyoming, USA.," *Journal of Petroleum Geology*, vol. 9, no. 4, pp. 393–411, 1986.

[18] J. C. Pratsch, "Focused gas migration and concentration of deep gas accumulations, NW German basin," in *Geochemistry*, E. A. Beaumont and N. H. Foster, Eds., vol. 8, pp. 613–619, AAPG Treatise of Petroleum Geology, 1988.

[19] J.-C. Pratsch, "The location of major oil- and gasfields: examples from the Andean foreland," *Journal of Petroleum Geology*, vol. 17, no. 3, pp. 327–338, 1994.

[20] Ø. Sylta, "Modelling of secondary migration and entrapment of a multicomponent hydrocarbon mixture using equation of state and ray-tracing modelling techniques," *Geological Society, London, Special Publications*, vol. 59, pp. 111–122, 1991.

[21] L. Hermans, A. D. van Kuyk, F. K. Lehner, and P. S. Featerstone, "Modeling secondary hydrocarbon migration in Haltenbanken, Norway," in *Structural and Tectonic Modeling and its Applications to Petroleum Geology*, R. M. Larsen, H. Brekke, B. J. Larsen, and E. Talleraas, Eds., vol. 1, pp. 305–323, Norwegian Petroleum Society, Special Publication, 1992.

[22] L. Catalan, Fu Xiaowen, I. Chatzis, and F. A. L. Dullien, "An experimental study of secondary oil migration," *The American Association of Petroleum Geologists Bulletin*, vol. 76, no. 5, pp. 638–650, 1992.

[23] M. M. Thomas and J. A. Clouse, "Scaled physical model of secondary migration," *AAPG Bulletin*, vol. 79, pp. 19–29, 1995.

[24] D. H. Welte, T. Hantschel, B. P. Wygrala, K. S. Weissenburger, and D. Carruthers, "Aspects of petroleum migration modelling," *Journal of Geochemical Exploration*, vol. 69, no. 70, pp. 711–714, 2000.

[25] F. Hao, H. Zou, Z. Gong, and Y. Deng, "Petroleum migration and accumulation in the Bozhong sub-basin, Bohai Bay basin, China: significance of preferential petroleum migration pathways (PPMP) for the formation of large oilfields in lacustrine fault basins," *Marine and Petroleum Geology*, vol. 24, no. 1, pp. 1–13, 2007.

[26] F. Hao, H. Zou, X. Li, and J. Jiang, "Migration and occurrence of high wax oils in the Damintun Depression, Northeast, China: Implication for primary controls of petroleum migration pathways in heterogeneous carrier beds," *Journal of Petroleum Science and Engineering*, vol. 67, no. 3-4, pp. 105–115, 2009.

[27] J. A. Miles, "Secondary migration routes in the Brent sandstones of the Viking Graben and East Shetland Basin: evidence from oil residues and subsurface pressure data," *The American Association of Petroleum Geologists Bulletin*, vol. 74, no. 11, pp. 1718–1735, 1990.

[28] L. Rhea, M. Person, G. De Marsily, E. Ledoux, and A. Galli, "Geostatistical models of secondary oil migration within heterogeneous carrier beds: a theoretical example," *The American Association of Petroleum Geologists Bulletin*, vol. 78, no. 11, pp. 1679–1691, 1994.

[29] E. Bekele, M. Person, and G. De Marsily, "Petroleum migration pathways and charge concentration: a three-dimensional model: discussion," *AAPG Bulletin*, vol. 83, no. 6, pp. 1015–1019, 1999.

[30] E. B. Bekele, M. A. Person, B. J. Rostron, and R. Barnes, "Modeling secondary oil migration with core-scale data: Viking Formation, Alberta basin," *AAPG Bulletin*, vol. 86, no. 1, pp. 55–74, 2002.

[31] M. Fustic, B. Bennett, H. Huang, and S. Larter, "Differential entrapment of charged oil—new insights on McMurray Formation oil trapping mechanisms," *Marine and Petroleum Geology*, vol. 36, no. 1, pp. 50–69, 2012.

[32] G. S. Long, H. S. Shi, and J. Y. Du, "An analysis of creation conditions for Miocene stratigraphic and lithologic traps in Huizhou area, Pearl River Mouth Basin," *China Offshore Oil and Gas*, vol. 18, pp. 229–235, 2006 (Chinese).

[33] Z. Sun, D. Zhou, S. Wu et al., "Patterns and dynamics of rifting on passive continental margin from shelf to slope of the northern South China Sea: Evidence from 3D analogue modeling," *Journal of Earth Science*, vol. 20, no. 1, pp. 136–146, 2009.

[34] A. Briais, P. Patriat, and P. Tapponnier, "Updated interpretation of magnetic anomalies and seafloor spreading stages in the south China Sea: implications for the Tertiary tectonics of Southeast Asia," *Journal of Geophysical Research: Solid Earth*, vol. 98, no. B4, pp. 6299–6328, 1993.

[35] B. Taylor and D. E. Hayes, "Origin and history of the South China Sea basin," in *The Tectonic and Geologic Evolution of Southeast Asian Seas and Islands: Part 2*, vol. 27 of *Geophysical Monograph Series*, pp. 23–56, American Geophysical Union, Washington, D. C., 1983.

[36] J. Gao, S. Wu, K. McIntosh et al., "The continent-ocean transition at the mid-northern margin of the South China Sea," *Tectonophysics*, vol. 654, pp. 1–19, 2015.

[37] C. Huang, D. Zhou, Z. Sun, C. Chen, and H. Hao, "Deep crustal structure of Baiyun Sag, northern South China Sea revealed from deep seismic reflection profile," *Chinese Science Bulletin*, vol. 50, no. 11, pp. 1131–1138, 2005.

[38] J. Wu, *Study on hydrocarbon accumulation mechanism in Huizhou Sag [M.S. thesis]*, China University of Geosciences, Wuhan, China, 2010 (Chinese).

[39] J. Espitalié, J. L. Laporte, M. Madec et al., "Méthode rapide de caractérisation des roches mètres, de leur potentiel pétrolier et de leur degré d'évolution," *Revue de l'Institut Français du Pétrole*, vol. 32, no. 1, pp. 23–42, 1977.

[40] J. Z. Zhu, H. S. Shi, Y. Shu, J. Y. Du, J. Y. Wu, and J. L. Luo, "Organic maceral characteristics and hydrocarbon-generation potentials of sourde rocks in the Pearl River Mouth Basin," *Petroleum Geology & Experiment*, vol. 29, no. 3, pp. 301–306, 2007 (Chinese).

[41] B. P. Tissot, "Premieres données sur les mécanismes et la cinétique de la formation du pétrole dans les sediments," *Revue Institut Francais du Petrole*, vol. 24, pp. 470–501, 1969.

[42] M. L. Bordenave, J. Espitalir, P. Leplat, J. L. Oudin, and M. Vandenbroucke, *Applied Geochemistry*, M. L. Bordenave, Ed., Technip, Paris, France, 1993.

[43] C. R. Robison, L. W. Elrod, and K. K. Bissada, "Petroleum generation, migration, and entrapment in the Zhu 1 depression, Pearl River mouth basin, South China Sea," *International Journal of Coal Geology*, vol. 37, no. 1-2, pp. 155–178, 1998.

[44] S. Zhang, D. Liang, Z. Gong et al., "Geochemistry of petroleum systems in the eastern Pearl River Mouth Basin: Evidence for mixed oils," *Organic Geochemistry*, vol. 34, no. 7, pp. 971–991, 2003.

[45] N. Ma, D. J. Hou, H. S. Shi, and J. Z. Zhu, "Analysis of the main controlling factors of source rocks of Huizhou Sag in the Pearl

River Mouth Basin," *Journal of Northeast Petroleum University*, vol. 36, no. 3, p. pp, 2012.

[46] C. M. Chen, H. S. Shi, and S. C. Xu, *Forming process of the Tertiary reservoirs in the Pearl River Mouth Basin (East area)*, Science Press, Beijing, China, 2003.

[47] J. Peng, X. Pang, S. Xiao et al., "Secondary migration of hydrocarbons in the zhujiang formation in the huixi half-graben, pearl river mouth basin, south china sea," *Canadian Journal of Earth Sciences*, vol. 53, no. 2, pp. 189–201, 2016.

[48] P. Ungerer, F. Bessis, P. Y. Chenet et al., *Geological and Geochemical Models in Oil Exploration: Principles and Practical Examples. Petroleum Geochemistry and Basin Evaluation*, R. J. Murris and G. Demaison, Eds., vol. 35, American Association of Petroleum Geologists Memoir, 1984.

[49] J. G. Sclater and P. A. Christie, "Continental stretching: an explanation of the Post-Mid-Cretaceous subsidence of the central North Sea Basin," *Journal of Geophysical Research*, vol. 85, no. B7, pp. 3711–3739, 1980.

[50] P. Ungerer, J. Burrus, B. Doligez, P. Y. Chenet, and F. Bessis, "Basin evaluation by integrated two-dimensional modeling of heat transfer, fluid flow, hydrocarbon generation, and migration," *The American Association of Petroleum Geologists Bulletin*, vol. 74, no. 3, pp. 309–335, 1990.

[51] A. K. Burnham and J. J. Sweeney, "A chemical kinetic model of vitrinite maturation and reflectance," *Geochimica et Cosmochimica Acta*, vol. 53, no. 10, pp. 2649–2657, 1989.

[52] J. J. Sweeney and A. K. Burnham, "Evaluation of a simple model of vitrinite reflectance based on chemical kinetics," *The American Association of Petroleum Geologists Bulletin*, vol. 74, no. 10, pp. 1559–1570, 1990.

[53] A. S. Pepper and P. J. Corvi, "Simple kinetic models of petroleum formation. Part III: Modelling an open system," *Marine and Petroleum Geology*, vol. 12, no. 4, pp. 417–452, 1995.

[54] P. Ungerer, J. EspitaliΘ, F. Behar, and S. Eggen, "Modélisation mathématique des interactions entre craquage thermique et migration lors de la genèse du pétrole et du gaz," in *Comptes Rendus de l'Académie des Sciences*, vol. 307, Paris, France, 1988.

[55] B. Durand, P. Ungerern, A. Chiarelli, and J. L. Oudin, "Modelisation de la migration de l'huile. Application à deux exemples de bassins sedimentaires," in *Proceedings of the 11th World Petroleum congress*, pp. 3–15, London, UK, 1983.

[56] Y. Zhang, *Characteristics and main controlling factors of hydrocarbon accumulation in the Eogene of Huihou Depression [M.S. thesis]*, China University of Geosciences, Wuhan, China, 2011 (Chinese).

[57] S. S. Cui, J. X. He, S. H. Chen, H. B. Ju, and J. Cui, "Development characteristics of Pearl River Mouth basin and its geological conditions for oil and gas accumulation," *Journal of Natural Gas Geoscience*, vol. 20, pp. 384–391, 2009 (Chinese).

[58] H. F. Jia, *Erosion thickness recovery of the Palaeogene and basin prototype analysis of the Huizhou Sag, the Pearl River Mouth Basin [M. S. thesis]*, China university of geosciences, Wuhan, China, 2007 (Chinese).

[59] H. F. Jia, L. F. Mei, H. S. Shi, S. M. Yu, T. Peng, and W. Min, "Structural-sedimentary synthetic method for restoring denuded thickness in rift-subsidence basin," *Geophysical Prospecting for Petroleum*, vol. 48, no. 3, pp. 314–318, 2009.

[60] Y. Li, Z. Jiang, S. Liang, J. Zhu, Y. Huang, and T. Luan, "Hydrocarbon generation in the lacustrine mudstones of the wenchang formation in the Baiyun Sag of the Pearl River Mouth Basin, Northern South China Sea," *Energy & Fuels*, vol. 30, no. 1, pp. 626–637, 2016.

[61] Z. Jiang, H. Du, Y. Li, Y. Zhang, and Y. Huang, "Simulation of gas generation from the paleogene enping formation in the baiyun sag in the deepwater area of the pearl river mouth basin, the South China Sea," *Energy & Fuels*, vol. 29, no. 2, pp. 577–586, 2015.

[62] Y. Yuan, W. Zhu, L. Mi, G. Zhang, S. Hu, and L. He, "'Uniform geothermal gradient' and heat flow in the Qiongdongnan and Pearl River Mouth Basins of the South China Sea," *Marine and Petroleum Geology*, vol. 26, no. 7, pp. 1152–1162, 2009.

[63] L. He, K. Wang, L. Xiong, and J. Wang, "Heat flow and thermal history of the South China Sea," *Physics of the Earth and Planetary Interiors*, vol. 126, no. 3-4, pp. 211–220, 2001.

[64] Y. S. Yuan, *Tectono-thermal evolution and source rock maturation history in deepwater area in the northern margin of the South China Sea [Ph.D thesis]*, Institute of Geology and Geology and Geophysics, Chinese Academy of Sciences, Beijing, China, 2007 (Chinese).

[65] Y. Li, X. Luo, X. Xu, X. Yang, and X. Shi, "Seafloor in-situ heat flow measurements in the deep-water areas of the northern slope, South China Sea," *Chinese Journal of Geophysics*, vol. 53, no. 5, pp. 774–783, 2010.

[66] X. Y. Tang, S. B. Hu, G. C. Zhang et al., "Characteristic of surface heat flow in the Pearl River Mouth Basin and its relationship with thermal lithosphere thickness," *Chinese Journal of Geophysics*, vol. 57, no. 6, pp. 1857–1866, 2014 (Chinese).

[67] X. Y. Tang, S. P. Huang, S. C. Yang, G. Z. Jiang, and S. B. Hu, "Correcting on Logging-derived temperatures of the Pearl River Mouth Basin and characteristics of its present temperature field," *Chinese Journal of Geophysics*, vol. 59, no. 8, pp. 2911–2921, 2016 (Chinese).

[68] X. W. Guo and S. He, "Source rock thermal and maturity haistory modeling in the Baiyun Sag of the Pearl River Mouth Basin," *Petroleum Geology & Experiment*, vol. 29, no. 4, pp. 420–425, 2007 (Chinese).

[69] J. Zhang, *Research on the numerical modeling of tectonic and geo-thermal history of rifted continental margin basin-a case study in deep water basin of the northern South China Sea [M.S. thesis]*, China University of Geosciences, Beijing, China, 2009 (Chinese).

[70] J. Shan, C. Q. Zhu, M. Xu, and S. B. Hu, "Tectonic-thermal evolution of the Northern margin of the South China Sea," in *Proceedings of the the Proceedings of the 25th annual meeting of the Chinese geophysical society*, 2009 (Chinese).

[71] B. A. Allen and J. R. Allen, *Basin Analysis: Principle and Applications*, Blackwell Scientific Publications, Oxford, London, 1990.

[72] A. H. E. Röhm, R. Snieder, S. Goes, and J. Trampert, "Thermal structure of continental upper mantle inferred from S-wave velocity and surface heat flow," *Earth and Planetary Science Letters*, vol. 181, no. 3, pp. 395–407, 2000.

Journal of
Geochemistry

Scientifica

International Journal of
Ecology
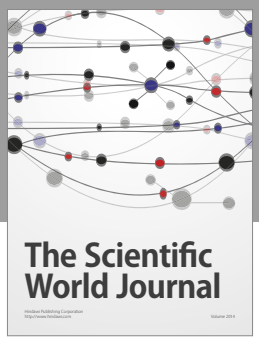
The Scientific
World Journal
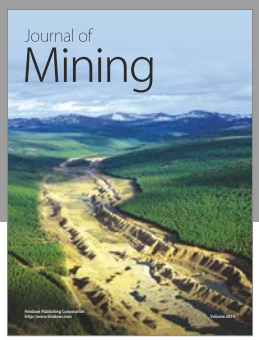
Journal of
Mining

Journal of
Earthquakes

Paleontology Journal
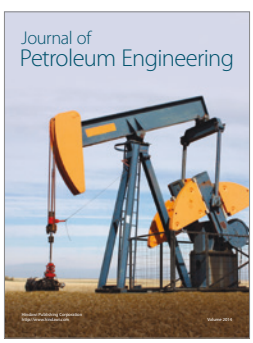
Journal of
Petroleum Engineering

Hindawi
Submit your manuscripts at
https://www.hindawi.com
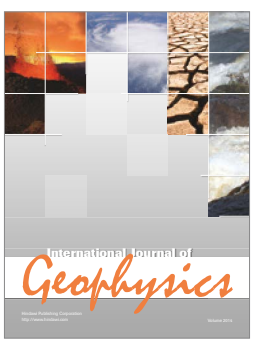
International Journal of
Geophysics
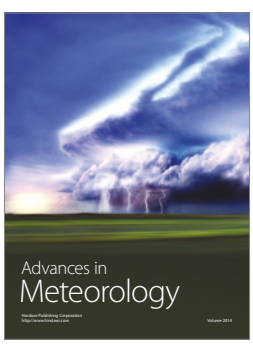
Advances in
Meteorology

Journal of
Climatology
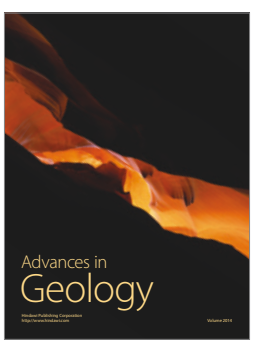
Advances in
Geology
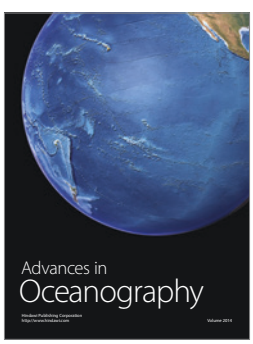
Advances in
Oceanography
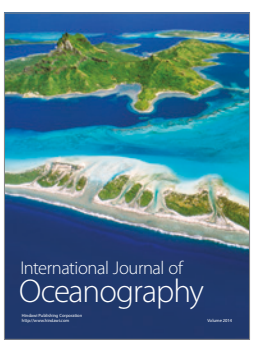
International Journal of
Oceanography
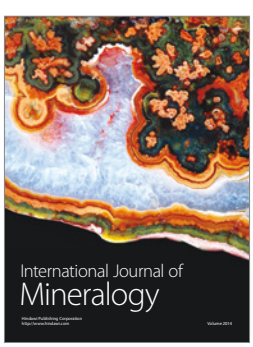
International Journal of
Mineralogy

Journal of
Geological Research

International Journal of
Atmospheric Sciences

Applied &
Environmental
Soil Science
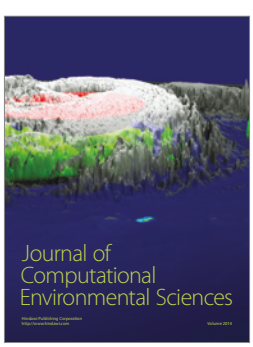
Journal of
Computational
Environmental Sciences